Impacts of Interactive Stratospheric Chemistry on Antarctic and Southern Ocean Climate Change in the Goddard Earth Observing System – Version 5 (GEOS-5)

Feng Li*

Goddard Earth Sciences Technology and Research, Universities Space Research Association, Columbia, Maryland, USA

Atmospheric Chemistry and Dynamics Laboratory, NASA Goddard Space Flight Center, Greenbelt, Maryland, USA

Yury V. Vikhliaev

Goddard Earth Sciences Technology and Research, Universities Space Research Association, Columbia, Maryland, USA

Global Modeling and Assimilation Office, NASA Goddard Space Flight Center, Greenbelt, Maryland, USA

Paul A. Newman

Atmospheric Chemistry and Dynamics Laboratory, NASA Goddard Space Flight Center, Greenbelt, Maryland, USA

Steven Pawson

Global Modeling and Assimilation Office, NASA Goddard Space Flight Center, Greenbelt, Maryland, USA

Judith Perlwitz

Cooperative Institute for Research in Environmental Sciences, University of Colorado, and Physical Sciences Division, NOAA/Earth System Research Laboratory, Boulder, Colorado, USA

Darryn W. Waugh

Department of Earth and Planetary Science, Johns Hopkins University, Baltimore, Maryland, USA

Anne R. Douglass

Atmospheric Chemistry and Dynamics Laboratory, NASA Goddard Space Flight Center, Greenbelt, Maryland, USA

---

*Corresponding author address: Feng Li, Atmospheric Chemistry and Dynamics Laboratory, NASA Goddard Space Flight Center, Greenbelt, Maryland, USA

E-mail: Feng.Li@nasa.gov

Abstract

Stratospheric ozone depletion plays a major role in driving climate change in the Southern Hemisphere. To date, many climate models prescribe the stratospheric ozone layer's evolution using monthly and zonally averaged ozone fields. However, the prescribed ozone underestimates Antarctic ozone depletion and lacks zonal asymmetries. In this study we investigate the impact of using interactive stratospheric chemistry instead of prescribed ozone on climate change simulations of the Antarctic and Southern Ocean. Two sets of 1960-2010 ensemble transient simulations are conducted with the coupled ocean version of the Goddard Earth Observing System Model version 5: one with interactive stratospheric chemistry and the other with prescribed ozone derived from the same interactive simulations. The model's climatology is evaluated using observations and reanalysis. Comparison of the 1979-2010 climate trends between these two simulations reveals that interactive chemistry has important effects on climate change not only in the Antarctic stratosphere, troposphere and surface, but also in the Southern Ocean and Antarctic sea ice. Interactive chemistry causes stronger Antarctic lower stratosphere cooling and circumpolar westerly acceleration during November-December-January. It enhances stratosphere-troposphere coupling and leads to significantly larger tropospheric and surface westerly changes. The significantly stronger surface wind-stress trends cause larger increases of the Southern Ocean Meridional Overturning Circulation, leading to year-round stronger ocean warming near the surface and enhanced Antarctic sea ice decrease.

1 Introduction

Numerous observational and modeling studies have established the essential role of Antarctic ozone depletion in driving Southern Hemisphere (SH) climate change in the last 3-4 decades (see reviews by Thompson et al. 2012 and Previdi and Polvani 2014, and the references therein). The ozone hole causes strong cooling of the Antarctic lower stratosphere in the austral late spring and summer (Shine 1986; Randel and Wu 1999), leading to a stronger and more persistent Antarctic polar vortex (Waugh et al. 1999). These stratospheric climate trends have significant impacts on the SH tropospheric circulation, driving the Southern Annual Mode (SAM) toward a more positive polarity (Thompson and Solomon 2002; Perlwitz et al. 2008). Changes in the SH extratropical sea level pressure, surface temperature, precipitation, and tropospheric and surface westerlies are all closely linked to this positive SAM trend (Thompson et al. 2012; Previdi and Polvani 2014). The ozone hole is also an important driver of Southern Ocean change, e.g., the spin up of the SH subtropical gyres (Cai 2006), strengthening of the meridional overturning circulation (Sigmond and Fyfe 2010; Sigmond et al. 2011; Solomon et al. 2015), and warming of the Southern Ocean (Sigmond and Fyfe 2010; Solomon et al. 2015).

Because the ozone hole plays a key role in driving recent SH climate change, it is important to realistically represent the stratospheric ozone climate forcing in climate models. Currently two very different approaches are used to represent ozone forcing. The first approach prescribes the stratospheric ozone evolution using monthly and

93 zonally averaged ozone fields. This method is easy to implement and is used in many
94 coupled atmosphere-ocean general circulation models (AOGCMs), including those
95 participating in the Coupled Model Intercomparison Project (CMIP). The second
96 approach is to calculate stratospheric ozone interactively with comprehensive
97 stratospheric chemistry - employed in the coupled chemistry-climate models (CCMs)
98 (Eyring et al. 2006). CCMs capture the interactions of dynamical, radiative, and chemical
99 processes and have been major tools for assessing ozone layer past changes and future
100 projections (SPARC CCMVal 2010).
101
102 Climate models with prescribed ozone appear to simulate well the observed climate
103 change over Antarctica (e.g. Gillett et al. 2003). However, the prescribed monthly-mean
104 and zonal-mean ozone fields do not fully capture two important aspects of the ozone
105 hole. First, prescribed ozone underestimates the magnitude of Antarctic ozone depletion
106 (Sassi et al. 2005; Neely et al. 2014). This bias is caused by temporal smoothing due to
107 the interpolation of monthly-mean values to determine ozone concentrations at each time
108 step. Second, the prescribed zonal-mean ozone lacks zonal asymmetries. The ozone hole
109 has a large wave-1 structure with its center usually located slightly away from the South
110 Pole towards the Atlantic Ocean (Grytsai et al. 2007). Lacking zonal asymmetries and
111 dynamical consistency in the prescribed ozone fields affects Rossby wave propagation
112 and stratospheric wave driving (Gabriel et al. 2007; Crook et al. 2008). The deficiencies
113 of the prescribed ozone affect simulated SH climate and climate change (Sassi et al.
114 2005; Crook et al. 2008; Gillett et al. 2009; Waugh et al. 2009; Neely et al. 2014). These
115 studies used different models and methods, but they all found similar results: prescribed

ozone simulations have weaker Antarctic lower stratosphere cooling than interactive chemistry simulations. Waugh et al. (2009) and Neely et al. (2014) further showed that these prescribed ozone simulations underestimate the Antarctic tropospheric circulation trends such as the poleward strengthening of the tropospheric westerlies.

The purpose of this study is to understand the effects of using interactive stratospheric chemistry instead of prescribed ozone on simulated Antarctic and Southern Ocean climate change. This is the first time the influences of interactive stratospheric chemistry on Southern Ocean and Antarctic sea ice have been studied. We perform and compare two transient simulation ensembles over 1960-2010 using the Goddard Earth Observing System Model version 5 (GEOS-5): one with interactive stratospheric chemistry and the other with prescribed ozone.

Descriptions of GEOS-5 and its chemistry schemes, experiment design, and simulations are given in section 2. In Section 3 we evaluate the model climatology with a focus on SH simulations for the 1990-2010 period using satellite observations and reanalysis data. The effects of interactive chemistry on Antarctic and Southern Ocean climate change are presented in section 4. Discussion and conclusions are given in section 5.

2 Model and Simulations

2.1 GEOS-5

We use a coupled ocean version of GEOS-5. The atmosphere model is GEOS-5 Fortuna (Molod et al. 2012) and the ocean model is the Modular Ocean Model version 4p1 (MOM4p1, Griffies et al. 2009). GEOS-5 Fortuna has 72 levels with a top at 0.01 hPa and MOM4p1 has 50 layers. The atmosphere model horizontal resolution is 2.5° longitude × 2° latitude. The ocean model resolution is 1° longitude × 1° latitude. A brief description of GEOS-5 Fortuna and MOM4p1 is given in the Appendix.

GEOS-5 includes two chemistry mechanisms: a comprehensive stratospheric chemistry model and a simple parameterized chemistry scheme.

1) Interactive Chemistry

The GEOS Chemistry-Climate Model (GEOSCCM) includes a comprehensive stratospheric chemistry model (Pawson et al. 2008; Oman and Douglass 2014). All of the important stratospheric gas phase and heterogeneous reactions are included in this chemistry module (Douglass and Kawa 1999; Considine et al. 2000). The stratospheric chemistry is coupled with physical processes through the radiation where radiatively important stratospheric trace species are calculated from the chemistry model. Results from the GEOSCCM have been extensively analyzed and evaluated using observation-based process-oriented diagnostics in the Stratosphere-troposphere Processes And their Role in Climate (SPARC) Chemistry Climate Model Validation - 2 Project (SPARC CCMVal 2010). Overall the GEOSCCM performs very well in comparison to observed stratospheric dynamical, chemical, and transport processes (SPARC CCMVal 2010; Strahan et al. 2011; Douglass et al. 2012).

2) Parameterized Chemistry

GEOS-5's default chemistry is a simple parameterization that prescribes monthly and zonally averaged fields for seven radiatively active trace species: odd oxygen (O_x), methane (CH_4), nitrous oxide (N_2O), water vapor (H_2O), CFC-11 (CCl_3F), CFC-12 (CCl_2F_2), and HCFC-22 ($CHClF_2$). These prescribed fields are obtained from interactive chemistry simulations. The prescribed zonal-mean, monthly-mean values are set as the middle-month values, and linearly interpolated to each time step. Ozone (O_3) is treated differently from the other species because it has a large mesospheric diurnal cycle that cannot be resolved from interpolation of monthly-mean values. In the stratosphere (pressures greater than 1 hPa), all O_x is O_3. In the mesosphere (pressures less than 1 hPa), O_3 is partitioned to approximate a diurnal cycle: at nighttime O_3 is O_x, but during daytime O_3 is reduced by a factor of $\exp[-1.5(\log_{10}p)^2]$ to approximate the daytime O_3 destruction, where p is pressure. The exponential damping factor of daytime O_3 is derived from interactive chemistry simulations. The O_x derived O_3 and the six other radiative species are used by the radiation code.

2.2 Experiment Design

In order to investigate the impacts of interactive stratospheric chemistry on Antarctic and Southern Ocean climate change in GEOS-5, we perform two sets of ensemble transient simulations of the 1960-2010 period. The first ensemble is from the GEOS coupled Atmosphere-Ocean-Chemistry Climate Model (AOCCM), i.e., with coupled ocean and

185 interactive stratospheric chemistry (hereafter referred to as interactive chemistry, or
186 interactive simulations). The second ensemble is from the GEOS-5 AOGCM, i.e., with
187 coupled ocean and parameterized chemistry (hereafter referred to as prescribed ozone, or
188 prescribed simulations). These two ensemble sets are forced with the same Chemistry
189 Climate Model Validation Project (CCMVal) REF1 scenarios for greenhouse gases
190 (GHGs) and ozone-depleting substances (ODSs). The only difference between the two
191 ensemble sets is the stratospheric chemistry representation.
192
193 Each ensemble set has four members and each member only differs in initial conditions.
194 We initially spin-up the ocean with a 200-year baseline simulation under perpetual 1950
195 conditions with the GEOS-5 AOGCM. We then perform one transient simulation from
196 1950 to 2010 with the GEOS AOCCM - the first member of the interactive simulations.
197 The other three interactive simulation members start on January 1, 1960, with initial
198 conditions from January 1 of 1959, 1961, and 1962 of the first member, respectively. The
199 four prescribed simulation members start on January 1, 1960, with initial conditions and
200 monthly-mean zonal-mean fields of the seven stratospheric radiative species taken from
201 their corresponding members of the interactive simulations. The ensemble-mean results
202 are presented in this study. Linear trends are calculated from the ensemble average of
203 model data of all four members. We also carry out an additional 100-year time-slice
204 simulation with the GEOS AOCCM under perpetual 1960 conditions. This control
205 simulation is used to correct the ocean and sea ice trends in both the interactive and
206 prescribed simulations due to climate drift, assuming that the drift in both simulations is
207 similar in 1960 conditions.

208

209 **3 Evaluation of model 1990-2010 climatology in the Interactive Chemistry**
210 **Simulations**

211

212 In this section we evaluate the climatology for the 1990-2010 period obtained from the
213 interactive chemistry simulations with emphasis on the Antarctica. We choose the 1990-
214 2010 period in order to compare model climatology with available satellite observations
215 and reanalysis data. The purposes are to identify model biases and to compare GEOS-5
216 performances with other climate models.

217

218 Total column ozone is a primary diagnostic for assessing stratospheric chemistry and
219 transport processes. Figure 1 compares GEOS AOCCM simulations with observed zonal-
220 mean total column ozone from the NASA merged Solar Backscatter Ultraviolet/Total
221 Ozone Mapping Spectrometer (SBUV/TOMS) data (no observations during polar night).
222 The model captures very well the observed total ozone seasonal and latitudinal structure,
223 e.g., the austral spring Antarctic ozone hole, the boreal spring Arctic ozone maximum,
224 and the tropical ozone minimum. The strength of the simulated Antarctic ozone hole
225 agrees with the observations. The model has slightly low biases in the tropics and high
226 biases in the extratropics, suggesting that the model may have a stronger Brewer-Dobson
227 circulation than the real atmosphere. Overall simulations of the stratospheric chemistry
228 and transport in the GEOS AOCCM are similar to those in the GEOSCCM, which have
229 been thoroughly evaluated and validated (Strahan et al. 2011; Douglass et al. 2012).

230

231 The seasonal evolution of Antarctic temperatures and zonal winds is well simulated.
232 Simulated Antarctic zonal-mean temperatures (65-90°S) and circumpolar zonal-mean
233 zonal winds (55-70°S) are compared to NASA Modern-Era Retrospective Analysis for
234 Research and Application reanalysis (MERRA, Rienecker et al. 2011) in Figure 2. In the
235 lower stratosphere, the model has warm biases in the austral winter and cold biases in the
236 austral spring (Figure 2b). The magnitude of the Antarctic temperature errors is within
237 the range in the CCMVal-2 models (Eyring et al. 2006). In general the simulated
238 circumpolar zonal winds have westerly biases (Figure 2d). The largest westerly biases are
239 found in spring, which is associated with the model spring "cold-pole" error. The model
240 Antarctic polar vortex persists longer and breaks up later and higher than observed. The
241 spring "cold-pole" and late polar vortex break up are longstanding biases in the middle
242 atmosphere models (Eyring et al. 2006), which are possibly due to missing orographic
243 gravity wave drag around 60°S in the models (McLandress et al. 2011). Coupling with
244 chemistry and ocean does not appear to reduce these biases.
245
246 The simulated tropospheric jet has a near barotropic structure and is centered at ~ 55°S
247 (Figure 2e). The model has westerly biases poleward of 50°S and easterly biases
248 equatorward of 50°S (Figure 2f). This dipole pattern means that the simulated
249 tropospheric jet is too close to the pole, which is associated with the year-round cold pole
250 biases in the troposphere (Figure 2b).
251
252 Surface wind-stress plays a key role in the coupled atmosphere-ocean climate system. It
253 is a major driver of the ocean circulation, and it also significantly affects the structure of

254 sea surface temperature, sea level, and Ekman transport. Figure 3a shows the simulated
255 annual-mean zonal wind-stress climatology. The zonal wind-stress is mostly easterly in
256 the tropics and subtropics, and westerly in the extratropics, reflecting the surface zonal
257 wind pattern. The most prominent feature in Figure 3a is the zonally-coherent westerly
258 maxima in the 40°–65°S latitudinal band. This powerful surface forcing is important in
259 driving the Antarctic Circumpolar Current (ACC), which has profound implications on
260 the Southern Ocean Meridional Overturning Circulation (MOC). The strength and
261 location of the simulated peak westerly wind-stress over the Southern Ocean greatly
262 influence simulations of the Southern Ocean (Russell et al. 2006).
263
264 We use satellite measurements and reanalysis data to assess the simulated surface wind-
265 stress climatology. The satellite measurements are from NASA Quick Scatterometer
266 (QuikSCAT), which provided 11 years' (September 1999 – October 2009) wind-stress
267 observations. The reanalysis data we use is the average of four datasets: MERRA, the
268 National Centers for Environmental Prediction – National Center for Atmospheric
269 Research (NCEP-NCAR) Global Reanalysis 1 (Kalney et al. 1996), NCEP-Department of
270 Energy (DOE) Reanalysis 2 (Kanamitsu et al. 2002), and the European Centre for
271 Medium-Range Weather Forecast Interim Re-Analysis (ERA-Interim, Dee et al. 2011).
272 Figure 3b shows the map of the differences between GEOS AOCCM and QuikSCAT
273 observations. In general the simulated zonal wind-stress has easterly biases in the low and
274 middle latitudes and westerly biases in the high latitudes. In the SH, the model biases
275 have a dipole structure with westerly and easterly biases poleward and equatorward of ~
276 50°S, respectively. These biases are consistent with those in the tropospheric jet (Figure

277 2f). Figure 3c compares the zonal-mean wind-stress climatology in the SH between the
278 model, QuikSCAT, and the reanalysis. The model does not represent the location and
279 strength of the maximum westerly over the Southern Ocean. The simulated peak westerly
280 wind-stress is located 4° southward of the peak latitude in QuikSCAT and the reanalysis.
281 The simulated peak magnitude is 25% stronger than the QuikSCAT, although it is only
282 slighter larger than the maximum in the reanalysis. The biases in the surface wind-stress's
283 latitudinal structure are consistent with those in the tropospheric jet (Figure 2f). We want
284 to point out that GEOS-5 simulated wind-stress climatology is comparable to the CMIP
285 models, almost all of which perform poorly on the location and strength of the maximum
286 westerly over the Southern Ocean (Swart and Fyfe 2012; Lee et al. 2013).
287
288 We should keep in mind that reanalysis data are not observations. Derived diagnostics in
289 the reanalysis such as surface wind-stress are not constrained by observations and could
290 have large errors. Figure 3c shows that while reanalysis data agree with QuikSCAT in the
291 location of the maximum westerly, they have consistent westerly biases between 30° and
292 60°S. The wind-stress climatology in the four reanalysis datasets agrees well with each
293 other (not shown), but the wind-stress trends are very different among the four datasets
294 (Swart and Fyfe 2012). This will be discussed in more detail in the next section.
295
296 Figure 4 shows the simulated annual-mean sea surface temperature (SST) and sea surface
297 salinity (SSS) climatology and their differences from observations. Compared with the
298 Reynolds SST analysis (Reynolds et al. 2002), the model tends to have warm biases in
299 the low latitudes and cold biases in the high latitudes. Large positive errors are found off

300 the west coast of the tropical North America, South America, and Africa. These are
301 common errors in climate models, which are partly due to weak coastal upwelling in
302 these regions (Griffies et al. 2009). They are also closely related to the biases in the
303 surface cloud radiative forcing. The simulated eastern Pacific/Atlantic stratus cloud decks
304 are not attached to the coast, but are displaced to the west, giving warm errors near the
305 coast and cold errors over subtropical gyres (Molod et al. 2012). This is also a common
306 deficiency in the CMIP models (Laura and Hamilton 2013; Calisto et al. 2014). The
307 largest SST errors are in the North Atlantic, which are caused primarily by a very weak
308 Atlantic Meridional Overturning Circulation (AMOC) in the model. The weak AMOC
309 leads to weak poleward heat transport to the North Atlantic and large cold biases in that
310 region. The weak AMOC and the associated large North Atlantic SST errors are serious
311 issues. There is ongoing research to address these issues.
312
313 The model simulates well the SSS over the Southern Ocean except near the Antarctic
314 continent and South America where the model has positive salinity errors in comparison
315 to the Levitus SSS data (Levitus 1982). The model tends to have fresh biases in regions
316 of low salinity, e.g., the tropical west and southwest Pacific and tropical Indian Ocean.
317 Large positive SSS errors are found in the Arctic, a common bias in the AOGCMs (e.g.
318 Delworth et al. 2006). In the North Atlantic the large fresh bias is related to the weak
319 AMOC. Other primary sources for the salinity bias are wrong precipitation patterns, river
320 discharge that is not well diffused, and parameterization of exchange with marginal seas.
321

322 The Southern Ocean MOC is particularly efficient in exchange of heat and carbon
323 between the surface and the deep ocean (Marshall and Speer 2012), and hence it plays an
324 essential role in modulating regional and global climate. The MOC can be divided into a
325 mostly wind-driven Eulerian circulation and an eddy circulation. Figures 5 shows the
326 annual-mean Eulerian and eddy MOC streamfunction. The Eulerian MOC includes a
327 clockwise upper cell (40°-65°S, 0-3000m), a counter-clockwise lower cell (30°-55°S,
328 2500-4500m), and another counter-clockwise cell south of 65°S. There are no
329 observations of the Southern Ocean MOC, but the structure and strength of the Eulerian
330 MOC shown in Figure 5 are similar to those reported in the CMIP3 (Sen Gupta et al.
331 2009) and CMIP5 (Downes and Hogg 2013) models. The eddy circulation is
332 parameterized using the Gent and McWilliams (1990) scheme, because the coarse
333 resolution of the ocean model cannot resolve fine-scale ocean eddies. The parameterized
334 eddy circulation tends to have the opposite sign of the Eulerian circulation, but is much
335 weaker than the Eulerian circulation. The maximum strength of the eddy MOC is 6
336 Sverdrups, whereas the strength of the Eulerian upper cell is 36 Sverdrups. Therefore the
337 net, or the residual, MOC is dominated by the Eulerian component in the SH extratropics.
338 For reference, the strength of the eddy MOC in the CMIP5 models ranges from 7 to 20
339 Sverdrups (Downes and Hogg 2013). Thus the eddy MOC in GEOS-5 is weaker than, but
340 comparable to the CMIP5 models.
341
342 Antarctic sea ice has a large seasonal cycle with minimum and maximum coverage in
343 February and September, respectively. The simulated seasonal cycle of the Antarctic sea
344 ice extent (SIE) is compared to the National Snow and Ice Data Center observations in

Figure 6. The model simulates well the timing and magnitude of the February SIE minimum and the recovery of the Antarctic sea ice from March to August. However, the simulated SIE maximum occurs in August, one month before the observed maximum in September. These results are within the large spread of Antarctic SIE in the CMIP5 models (Turner et al. 2013).

In summary, GEOS AOCCM reasonably simulates the Antarctic and Southern Ocean climatology. Overall this model's performance is comparable to current start-of-the-art climate models.

4 Impacts of Interactive Chemistry on Climate Change in the Antarctic and Southern Ocean

The interactive and prescribed simulations have different zonal-mean ozone climatology. Figure 7a compares the Antarctic (65°-90°S) total ozone seasonal cycle between TOMS/SBUV, the interactive and the prescribed runs. In October, the interactive simulations have a 207 DU ozone hole, while the prescribed simulations are 217 DU, and the observed October total ozone is 210 DU. The 10 DU ozone hole differences between the two simulations are caused by temporal smoothing of the parameterized chemistry. The parameterized chemistry sets the prescribed monthly-mean ozone from the interactive runs as the middle-month value, then interpolates linearly to determine ozone concentrations at every time step. This method is commonly used in other non-interactive chemistry models (Sassi et al. 2005; Neely et al. 2014). The problem with this method is

368 that it acts to temporally smooth the monthly variations and thus underestimates the
369 magnitude of the maximum/minimum monthly-mean ozone values in the interactive runs,
370 resulting in high ozone biases in October when ozone reaches minimum.
371
372 Another major deficiency of the prescribed simulations is the lack of ozone zonal
373 asymmetries. A related issue is that the prescribed ozone is not dynamically consistent
374 with the stratospheric circulation. In the interactive simulations Antarctic ozone exhibits
375 maximum zonal asymmetries during austral spring when the ozone hole forms (Figure
376 7b). In general the ozone hole is offset from the South Pole toward the west Antarctica
377 and the southern Atlantic Ocean, reflecting the influence of planetary waves (Grytsai et
378 al. 2007). Large ozone zonal asymmetries are also found in February and March, which is
379 associated with a large wave-1 structure in the geopotential height. Previous studies have
380 shown that lacking zonal asymmetries and dynamical consistency affects the
381 stratospheric circulation and even the tropospheric climate trends (Crook et al. 2008;
382 Waugh et al. 2009).
383
384 Ozone biases in the prescribed runs affect simulations of Antarctic stratosphere
385 temperatures. Figure 8a shows that the interactive simulations tend to have lower
386 temperatures in winter and spring and higher temperatures in summer and fall than the
387 prescribed simulations. Shading indicates that the differences (interactive minus
388 prescribed) are statistically significant at the 5% level based on a two-sample t-test. The
389 patterns of temperature differences do not exactly match those of ozone differences
390 (Figures 8a-b), e.g., the cooling in the lower stratosphere during austral winter and the

391 warming near 200 hPa during February-March-April-May. This indicates that radiative
392 forcing is not the sole factor driving temperature differences. Figures 8c and 8d show
393 differences in the dynamical and shortwave heating rates, respectively. The magnitude of
394 dynamical heating differences is comparable to or even stronger than that of shortwave
395 heating differences. Comparing Figures 8a and 8c clearly shows that the cooling in June-
396 July-August and the 200 hPa warming during February-March-April-May are driven by
397 dynamical heating changes. Therefore, changes in the dynamics also play an important
398 role in driving temperature differences (Crook et al. 2008).
399
400 As expected, differences in the shortwave heating rates have the same pattern as ozone
401 differences except during the austral winter. The deeper October ozone hole in the
402 interactive runs (in the lower stratosphere in October in Figure 8b, also see Figure 7a)
403 absorbs less shortwave radiation, leading to a colder lower stratosphere in October and
404 November. Weaker dynamical heating in October (Figure 8c) could also contribute to the
405 lower stratospheric temperature differences in the late spring. Differences in dynamical
406 heating reflect the response of the stratospheric wave-driven Brewer-Dobson circulation
407 to interactive chemistry. They are associated with the lack of zonal asymmetries in the
408 prescribed ozone, which modulates stratospheric wave driving (Nathan and Cordero
409 2007; Crook et al. 2008). The ozone hole also induces dynamical feedback and increases
410 the downwelling in the Antarctic stratosphere in the austral late spring and summer
411 (Stolarski et al. 2006; Li et al. 2008). Thus the stronger dynamical warming that
412 propagates from the upper stratosphere in October and November to lower stratosphere in

December and January is also linked to the deeper ozone hole in the interactive simulations (Figure 8c).

Interactive ozone chemistry has important impacts on simulations of climate change over the Antarctica. Figures 9a-f compare linear trends of the Antarctic temperatures (65°-90°S) and the circumpolar zonal winds (55°-70°S) in 1979-2010. Shading in Figure 9 indicates that the trends are statistically significant from zero at the 2-tailed 95% confidence interval, where the confidence interval is calculated following Santer et al. (2000). Overall the interactive and prescribed simulations have similar patterns: cooling in the lower stratosphere and intensification of the stratospheric and tropospheric westerlies during the Austral spring and summer seasons. However, the trends are stronger in the interactive runs. The maximum stratospheric cooling trend at November and 70 hPa is 3.4 and 2.9 K/decade in the interactive and prescribed runs, respectively. The peak westerly acceleration in the interactive runs is ~ 30% stronger at 20 hPa and 70% stronger at 500 hPa than in the prescribed runs. Also the peak westerly trends in the troposphere occur one month earlier in the interactive runs (December) than in the prescribed runs (January).

The Antarctic temperature and zonal wind trends from MERRA are also shown in Figure 9. The MERRA trends are much noisier than the simulated trends particularly in the upper stratosphere. The maximum lower stratosphere cooling in MERRA is 3.1 K/decade, between that of the interactive and prescribed runs. We have also found that temperature trends calculated using the Radiosonde Innovation Composite

436 Homogenization dataset (Hamiberger et al. 2012) agree well with the MERRA trends in
437 the lower stratosphere (not shown). As for the circumpolar westerly accelerations, the
438 MERRA trends are smaller than both simulations in the stratosphere, but are between the
439 interactive and prescribed runs in the troposphere.
440
441 The lower stratospheric cooling is caused by the decrease of shortwave heating (Figures 9
442 g-h), which is partly compensated by an increase of dynamical warming (Figures 9 i-j).
443 The stronger cooling in the interactive simulations is mainly driven by stronger decrease
444 of shortwave heating (Figures 9 g-h), which originates from stronger ozone depletion.
445
446 At the surface, zonal wind trend in the interactive runs is statistically significant in
447 November-December-January (NDJ) (Figure 10). The trends in these three months are all
448 larger than those in the prescribed runs, although the trend differences are not statistically
449 significant. The NDJ-mean surface circumpolar westerly trend is 0.46 m/s/decade in the
450 interactive simulations, about 70% larger than in the prescribed simulations. It is
451 interesting to note that the relative differences of the circumpolar westerly trends amplify
452 from the stratosphere (about 30%) to the troposphere and surface (about 70%),
453 suggesting that interactive chemistry affects stratosphere-troposphere coupling. Hereafter
454 we will focus on the NDJ period when climate trends in the interactive and prescribed
455 runs have the largest differences.
456
457 Climate change in the SH middle and high latitudes during the past several decades is
458 closely related to the shift of the SAM toward its positive polarity (Thompson and

459 Solomon 2002). The shift of the SAM polarity is commonly illustrated as the poleward
460 intensification of the tropospheric westerlies (Figure 11). Both runs simulate a
461 statistically significant dipole structure of the tropospheric zonal-mean zonal wind trends
462 during NDJ with eastward acceleration centered at 65°S and westward acceleration
463 centered at 45°S. This dipole structure, a signature of the SAM shift, has a larger
464 magnitude in the interactive runs. For example, the maximum eastward and westward
465 trends at 300 hPa are respectively 1.25 and -0.8 m/s/decade in the interactive runs, which
466 are more than 100% stronger than in the prescribed runs.
467
468 The amplification of zonal wind response to interactive chemistry from stratosphere to
469 troposphere and surface is clearly seen in Figure 11. The relative difference of the
470 maximum westerly trend is about 20% in the stratosphere, and increases to more than
471 100% below 300 hPa. Neely el al. (2014) showed similar results (see their Figure 3), but
472 they did not discuss this effect. Noting that the trends in the interactive simulations are
473 always stronger, we use a 1-tailed t test to find out whether these differences are
474 statistically significant following the method of Wigley (2006). The trend differences are
475 not statistically significant in the stratosphere, but the interactive simulations have
476 significantly stronger westerly accelerations than the prescribed runs between about 60°S
477 and 70°S and from the surface to 200 hPa. We do not know what causes the enhanced
478 tropospheric response. Indeed how the ozone hole-induced lower stratospheric westerly
479 anomalies are propagated downward to the troposphere is not well understood (e.g.,
480 Thompson et al. 2012). Nevertheless, this amplified tropospheric response indicates a

481 stronger stratosphere-troposphere coupling and has important implications on surface
482 wind-stress and Southern Ocean changes.
483
484 We are particularly interested in the impacts of interactive chemistry on simulations of
485 the SH surface wind-stress. The strong westerly surface wind-stress over the Southern
486 Ocean directly affects Ekman transport and the meridional overturning circulation.
487 Through its impacts on the surface wind-stress, the stratospheric ozone chemistry could
488 affect Southern Ocean circulation. Figure 12a compares the NDJ zonal-mean surface
489 zonal wind-stress trends in the interactive (green) and prescribed (red) simulations. The
490 trends in both simulations have the same latitudinal structure with a westerly and an
491 easterly maximum centered at 62°S and 46°S, respectively. The maximum westerly and
492 easterly trends in the interactive runs are about two times larger (statistically significant
493 at the 5% level) than those in the prescribed runs, consistently with the significantly
494 stronger tropospheric and surface zonal wind trends in the interactive runs shown in
495 Figure 11.
496
497 A commonly used diagnostic for surface wind-stress change is the trend of the maximum
498 strength (Swart and Fyfe 2012). We use this diagnostic to evaluate how interactive
499 chemistry improves the simulation of wind-stress increase compared with the reanalysis
500 data. Figure 12b shows that the trend of the NDJ westerly wind-stress maximum in the
501 interactive runs is 60% larger than that in the prescribed runs. The trend in the interactive
502 simulations (0.005 Pa/decade) is still much smaller than the average trend of the four
503 reanalysis (0.009 Pa/decade). However, the reanalysis trends have large spread: the ERA-

504 Interim and MERRA do not have a statistically significant trend, and the NCEP-NCAR
505 and NCEP-DOE trends are more than twice the ERA-Interim trend. These larger
506 uncertainties in the reanalysis make it difficult to validate the improvements of interactive
507 chemistry on simulated surface wind-stress changes.
508
509 The larger increase of surface forcing in the interactive runs significantly affects the
510 simulated Southern Ocean circulation changes. A comparison of the NDJ trends in the
511 zonal-mean surface zonal and meridional currents is shown in Figure 13a-b. The westerly
512 and northerly trend maxima are about two times larger in the interactive runs than in
513 prescribed runs and these trend differences are statistically significant, consistent with the
514 differences in the surface wind-stress trends (Figure 12a). This similarity is due to the
515 direct dynamical effect of surface wind-stress on the surface Ekman transport. The trends
516 of the ocean currents, particularly the meridional current, decrease rapidly with depth
517 (Figures 13 c-f). The interactive runs simulate significantly larger westerly and northerly
518 trends poleward of about 55°S. The westerly current trend differences extend from
519 surface to the deep ocean (only the upper 100 meters are shown in Figures 13 c-d), but
520 the northerly current trends differences are limited to the upper 80 meters (Figures 13 e-
521 f).
522
523 Interactive chemistry has significantly impact on changes in the Southern Ocean MOC.
524 Figures 14 compares trends of the NDJ Eulerian MOC streamfunction. The trends are
525 dominated by a dipole structure, indicating a poleward shift and strengthening of the
526 upper cell. Similar trends have been reported in previous studies on the Southern Ocean

MOC changes (Sigmond and Fyfe 2010; Solomon et al. 2015). The latitudinal structure and magnitude of the MOC trends are determined by the surface wind-stress (Figure 12a). Consistent with larger surface wind-stress changes, the MOC trends in the interactive runs are larger than in the prescribed runs. The differences in the MOC trends reach to below 3000 m. Most of the significantly different trends are found in the upwelling branch of the MOC poleward of 60°S. We have described in Figure 5 that the parameterized eddy MOC is much weaker than the Eulerian MOC. Similarly, the trends of the eddy MOC are much smaller than those of the Eulerian MOC (not shown). This is true for both the interactive and prescribed simulations.

That the interactive runs produce a stronger increase of the Southern Ocean MOC could have important implications for simulated global climate change. For instance, an enhanced upwelling of carbon-rich deep Southern Ocean water will affect the global carbon cycle (Russell et al. 2006b; Lenton et al. 2009). It should be noted, however, that there are strong debates on how the Southern Ocean eddy circulation will respond to increases of the surface wind. Some eddy-resolving ocean models simulate much stronger eddy circulation increases than in the coarse-resolution models (Spence et al. 2010; Farneti et al. 2010). In these eddy-resolving simulations, the increases of the eddy MOC compensate a larger fraction of, or even balance, the increases of the Eulerian cell, resulting in little or no changes in the residual MOC. There is no direct observational evidence to confirm whether or not the MOC has increased. Some ocean properties affected by the MOC (e.g. ventilations) show changes consistent with an increase of the

549 MOC (Waugh et al. 2012), but other properties such as the slope of isopycnals do not
550 show changes (Boning et al. 2008).
551
552 The differences in the Southern Ocean trends between the interactive and prescribed runs
553 are largest during NDJ, indicating that on seasonal timescale there is no delay in the
554 ocean circulation's response to changes in the overlying surface forcing. In other seasons,
555 the interactive and prescribed simulations produce similar trends of the surface wind-
556 stress and MOC (not shown). However, the seasonal wind-stress differences have year-
557 round impacts on Southern Ocean temperature changes. Figures 15 a-b show the
558 climatology (contours) and trends (color shading) of the zonal-mean ocean temperature in
559 NDJ and May-June-July (MJJ) in the interactive runs. The ocean temperature trends are
560 corrected for model drift by subtracting the trends in the 100-year perpetual 1960 control
561 simulation. The ocean temperature drift in the control simulation is much smaller than the
562 forced changes in the interactive or prescribed simulations in most of the Southern Ocean
563 (not shown). In NDJ ocean warming is strongly affected by the enhanced Ekman
564 transport and strengthening of the MOC. At the surface the enhanced Ekman flow
565 transports cold ocean water equatorward south of 55°S and warm water poleward north
566 of 55°S (see Figure 13b). This leads to a very weak surface cooling at 64°S (not
567 statistically significant) and the largest warming at 45°S, which corresponds respectively
568 to the latitudes of the maximum northerly and southerly trends of the surface meridional
569 ocean currents (Figure 13b). The large warming at 45°S extends to the deeper ocean due
570 to strong Ekman pumping. Near the continent below about 100 m the ocean temperature
571 increases with depth, thus the strengthening of the MOC upwelling increases the upward

572 ocean heat transport, causing enhanced warming just below the weak surface cooling.
573 Changes in the Ekman transport and MOC are much weaker and not statistically
574 significant in other seasons (not shown). However, due to the larger thermal inertia of the
575 ocean, the overall pattern of ocean temperature trends in MJJ (Figure 15b) and other
576 seasons is similar to that in NDJ, although the near-surface dipole structure at 64°S
577 disappears in other seasons.
578
579 Contrasting ocean temperature changes between the interactive and prescribed runs
580 reveal some complicated structures (Figures 15 c-d). In NDJ the interactive runs have
581 significantly stronger warming in 60°-70°S and below 40 meters with maximum
582 warming about twice as large as in the prescribed runs, consistent with a stronger
583 increase of the MOC upwelling. Stronger cooling is found under the surface around 64°S
584 (not statistically significant), indicating stronger surface Ekman transport. But interactive
585 runs also show weaker warming below about 30 meters in 40°-50°S, suggesting
586 competing effects of the enhanced Ekman transport and MOC on ocean temperature
587 change in this region. In MJJ the interactive runs have significantly stronger warming
588 poleward of 55°S. Note that the edge of the Antarctic sea ice (approximately the 0 degree
589 isothermal in Figure 15) is located between 55° and 60°S. Thus there is stronger warming
590 under the sea ice in the interactive runs, which affects simulated Antarctic sea ice change.
591
592 Figure 16 compares the trends of the SIE in 1979-2010 (corrected for model drift based
593 on the 100-year perpetual 1960 control simulation). The SIE drift in the control
594 simulation is much smaller than the changes in the interactive and prescribed simulations

595 (not shown). Both runs simulate a decrease of Antarctic SIE, in contrast to the observed
596 Antarctic SIE increase for the past 30 years (Zwally et al. 2002). This is a common bias
597 in the CMIP models (Turner et al. 2013), although some studies have suggested that this
598 discrepancy might be caused by large internal variability of the Antarctic sea ice (Swart
599 and Fyfe 2013; Polvani and Smith 2013; Gagne et al. 2015). The interesting result here is
600 that the interactive runs have a year-round larger decrease than the prescribed runs, i.e.,
601 interactive chemistry leads to Antarctic SIE decrease. We have shown in Figure 15b that
602 interactive simulations have significantly stronger near-surface ocean warming
603 throughout the year, which causes enhanced year-round sea ice decrease. The SIE trend
604 differences, however, are not statistically significant. This is probably due to the SIE's
605 large variability and the relatively small ensemble members in our simulations.
606
607 The impacts of interactive stratospheric chemistry on Southern Ocean and Antarctic sea
608 ice are qualitatively very similar to the impacts of the ozone hole that was first reported
609 by Sigmond and Fyfe (2010). They found that, by increasing the summertime surface
610 wind-stress over the Southern Ocean, the ozone hole acts to increase the overturning
611 circulation, warm the upper ocean, and decrease the Antarctic sea ice. These ozone hole
612 effects have been shown to be robust in several recent studies (Sigmond et al. 2011; Bitz
613 and Polvani 2012; Sigmond and Fyfe 2014; Solomon et al. 2015). Our results support
614 these findings, particularly that the observed Antarctic sea ice increase is not caused by
615 ozone depletion.
616
617 **5 Discussion and Conclusions**

Stratospheric ozone depletion impacts on SH climate change are now well recognized. The most realistic way to represent stratospheric ozone forcing in climate models is to calculate ozone interactively, but current climate models commonly use prescribed monthly and zonally averaged ozone fields. The prescribed ozone fields underestimate the ozone hole forcing and lack zonal asymmetries. This study investigates how these deficiencies in the prescribed ozone affect simulations of recent climate change in the Antarctic and the Southern Ocean. Previous studies have focused on the effects of prescribed ozone on simulations of Antarctic atmosphere. Here, we also study – for the first time - the impacts on simulated changes in Southern Ocean circulation and Antarctic sea ice.

Two sets of ensemble transient simulations of 1960-2010 are conducted with GEOS-5, one with interactive stratospheric chemistry and the other with prescribed monthly- and zonal- mean ozone and six other radiatively active trace species. Radiative forcing in the stratosphere due to ozone is much more important than the other six species. Therefore differences in the simulated climate and trends between the two runs are attributed mostly to ozone differences.

The climatology from the interactive chemistry simulations is assessed with emphasis on the SH. Overall GEOS-5 simulates reasonably well the climatology of the Antarctic atmosphere, Southern Ocean circulation, and Antarctic sea ice. The model has a spring "cold pole" bias and the associated late vortex breakup. It does not correctly reproduce

641 the observed strength and location of the maximum surface westerly wind-stress. These
642 errors are very common in the current start-of-the-art climate models and need to be
643 improved in order to better understand climate change over the Antarctica.
644
645 We focus on the 1979-2010 climate trends differences between the interactive chemistry
646 and prescribed ozone simulations. The interactive runs have stronger cooling and
647 westerly acceleration in the Antarctic lower stratosphere during austral spring and
648 summer. The larger westerly trends in the interactive runs penetrate to the troposphere
649 and surface. These results are consistent with previous studies (Waugh et al. 2009; Neely
650 et al. 2014), although the largest trend differences between the interactive and prescribed
651 runs occur in NDJ, not in DJF as reported in those studies. Interestingly, the zonal wind
652 response to interactive chemistry increases from about 20-30% (not statistically
653 significant) in the lower stratosphere to more than 100% (statistically significant) in the
654 troposphere and surface. The maximum NDJ westerly surface wind-stress trend in the
655 interactive runs is twice as large in the prescribed runs.
656
657 The significantly different surface forcing in the two simulations has important effects on
658 changes in the Southern Ocean circulation, temperature, and Antarctic sea ice. The larger
659 surface wind-stress trends in the interactive runs drive significantly larger changes in the
660 NDJ Southern Ocean currents and MOC upwelling. The interactive chemistry impact on
661 the MOC extends below 3000 m. The different changes in the MOC affect warming of
662 the Southern Ocean. In NDJ, the stronger MOC upwelling in the interactive runs brings
663 more upward ocean heat flux to the near surface and causes stronger warming under the

664 sea ice. This Southern Ocean temperature warming difference persists throughout the
665 year due to the large ocean thermal inertia, resulting in year-round larger Antarctic sea
666 ice decrease in the interactive runs..
667
668 In conclusion, we find significant Southern Ocean responses to the interactive
669 stratospheric chemistry: increase of the overturning circulation in NDJ, year-round
670 warming of the near surface ocean, and decrease of the Antarctic SIE. These ocean
671 responses originate from a larger increase of the surface wind-stress in NDJ, which is due
672 to a stronger lower stratospheric cooling and enhanced stratosphere-troposphere coupling.
673 Our results are consistent with studies on the effects of the ozone hole on Southern Ocean
674 circulation, temperature, and Antarctic sea ice (Sigmond and Fyfe 2010; Sigmond et al.
675 2011; Bitz and Polvani 2012; Sigmond and Fyfe 2014; Solomon et al. 2015). Here we
676 show that the interactive stratospheric chemistry can increase the ozone hole effects by
677 up to 100% compared to prescribed ozone, highlighting the importance of correctly
678 representing stratospheric ozone forcing in climate model in order to fully capture its
679 effects on climate change.
680
681 The ozone hole is projected to recover in the latter half of the 21st century (Eyring et al.
682 2007) and the ozone impacts on the Southern Ocean and Antarctic sea ice are expected to
683 reverse. Smith et al. (2012) reported in a modeling study that ozone recovery causes
684 weaker summertime wind-stress, colder upper ocean temperature, and an increase of the
685 Antarctic sea ice that acts to mitigate future sea ice loss. The CMIP models appear to
686 capture the ozone recover effects on mitigating Antarctic sea ice decrease (Sigmond and

687 Fyfe 2014). The findings in this study suggest that these ozone recovery effects might be
688 significantly underestimated in models using prescribed ozone, which include most of the
689 CMIP3 and CMIP 5 models.
690
691 In our simulations, the climatology and trends of the parameterized ocean eddy
692 circulation are much weaker than those of the Eulerian mean circulation. Therefore the
693 response of the residual circulation to stronger surface forcing is dominated by the
694 increase of the Eulerian circulation. Some eddy-resolving ocean models simulate much
695 stronger eddy response to increase of the surface forcing than the coarse-resolution ocean
696 models do. But Bitz and Polvani (2012) found that responses of the Southern Ocean
697 temperature and Antarctic sea ice to ozone depletion are essentially the same in an eddy-
698 resolving and a coarse resolution ocean model. It remains to be seen whether our results
699 can be verified in fine resolution ocean simulations.
700
701 Sigmond et al. (2010) investigated the impact of atmosphere-ocean coupling on the SAM.
702 Their study found that atmosphere-ocean interactions increase the persistence of the
703 SAM, but they do not impact the forced SAM response to the ozone hole. This study
704 shows that coupling with interactive chemistry is necessary to correctly represent the
705 response of the SAM variability to stratospheric ozone forcing. Our results also help to
706 answer the question raised by Son et al. (2008, 2010) as why CCMs with interactive
707 chemistry simulate stronger SAM response to ozone depletion and recovery than the
708 CMIP4 models with prescribed ozone.
709

One important question that is not answered by this study is which aspect of the prescribed ozone deficiencies contributes most to the weaker trends in the prescribed runs: a weaker ozone hole forcing due to interpolation of monthly-mean values or lack of zonal asymmetries. Neely et al. (2014) compared simulations using prescribed daily zonal-mean ozone, monthly zonal-mean ozone, and interactive chemistry with the NCAR Community Earth System Model. They found that the daily-mean ozone simulations largely reduce biases in simulated SH climate and climate change in the monthly-mean ozone simulations, indicating that ozone zonal asymmetry is not an important factor in the NCAR model. However, such experiment needs to be repeated with other models to determine whether these findings based on the NCAR model are robust. Clearly more work is needed to fully understand the role of specific aspects of the ozone forcing.

Acknowledgements

This work is supported by NASA's Modeling, Analysis and Prediction Program (MAP), and Atmospheric Composition Modeling and Analysis Program (ACMAP). D.W.W. is funded, in part, by a grant from the U.S. National Science Foundation. Computational resources for this work were provided by NASA's High-Performance Computing though the generous award of computing time as NASA Center for Climate Simulation (NCCS) and NASA Advanced Supercomputing (NAS) Division. We thank three anonymous reviewers for their valuable comments.

Appendix

GEOS-5 Model

GEOS-5 is an Earth system model developed at National Aeronautics and Space Administration (NASA) Goddard Space Flight Center (GSFC). It integrates together the atmosphere, land, ocean, chemistry, aerosol, and sea ice models using the Earth System Modeling Framework (Hill et al. 2004). GEOS-5 is a flexible model system and it can be run with different modes, e.g., atmosphere only, coupled atmosphere-ocean, and coupled atmosphere-ocean with interactive chemistry.

GEOS-5 Atmospheric General Circulation Model (GEOS-5 AGCM) is the atmosphere only version of the GEOS-5. In this study we use the Fortuna tag of GEOS-5 AGCM, whose details are described in Molod et al. (2012). GEOS-5 Fortuna has a finite-volume dynamical core. Its atmospheric physics includes parameterization schemes for convection, larger scale precipitation and cloud cover, shortwave and longwave radiation, turbulence, gravity wave drag and a land surface model (Molod et al. 2012). GEOS-5 AGCM has 72 vertical levels with a model top at 0.01 hPa. The horizontal resolution is adjustable, but all simulations in this study use a resolution of 2.5° longitude by 2° latitude.

GEOS-5 AOGCM is the coupled ocean version of the GEOS-5. It couples GEOS-5 AGCM with the Modular Ocean Model (MOM) developed by the Geophysical Fluid Dynamics Laboratory (Griffies et al. 2005). The version of the MOM used in this study is

MOM4p1 (Griffies et al. 2009). The ocean model has 50 vertical levels with a fine resolution of 10 meters in the top 200 meters. MOM uses a tripolar grid with poles over Eurasia, North America, and Antarctica. The zonal resolution is 1°. The meridional resolution is 1° in the extratropics and increases from 1° at 30° latitudes to 1/3° at the equator. The MOM4p1 is not an eddy-resolving model and the eddy fluxes are parameterized using the Gent and McWilliams (1990) scheme. MOM4p1 include parameterization schemes for penetrative shortwave radiation, horizontal friction, convection, from drag arising from unresolved mesoscale eddies, tidal mixing, vertical mixing, and overflow (Griffies et al. 2009).

The atmosphere and ocean model components exchange fluxes of momentum, heat and fresh water through a "skin layer" interface. The skin layer includes the Los Alamos Sea Ice Model, CICE (Hunke and Lipscomb 2008). CICE computes ice growth and melt subject to energy exchange. It also computes ice drift. CICE interacts with atmosphere and ocean by exchanging momentum, energy and masses through stress and fluxes.

772 **References**

773

774 Bitz, C. M., L. M. Polvani, 2012: Antarctic climate response to stratospheric ozone
775 depletion in a fine resolution ocean climate model. *Geophys. Res. Lett*., **39**: L20705,
776 doi:10.1029/2012GL053393.

777

778 Böning, C. W., A. Dispert, M. Visbeck, S. R. Rintoul, and F. U. Schwarzkopf; 2008: The
779 response of the Antarctic Circumpolar Current to recent climate change. *Nature Geosci.*
780 **1**, 864–869.

781

782 Cai, W., 2006: Antarctic ozone depletion causes an intensification of the Southern Ocean
783 supergyre circulation. *Geophys. Res. Lett.,* **33**, L03712, doi:10.1029/2005GL024911.

784

785 Calisto, M., D. Folini, M. Wild, and L. Bengtsson, 2014: Cloud radiative forcing
786 Intercomparison between fully coupled CMIP5 models and CERES satellite data. *Ann.*
787 *Geophys*., **32**, 793-807.

788

789 Crook, J. A., N. P. Gillett, and S. P. E. Keeley, 2008: Sensitivity of Southern Hemisphere
790 climate to zonal asymmetry in ozone. *Geophys. Res. Lett.,* **35**, L07806,
791 doi:10.1029/2007GL032698.

792

793 Dee, D. P., and Coauthors, 2011: The ERA-Interim reanalysis: Configuration and
794 performance of the data assimilation system. *Q. J. R. Meteorol. Soc.,* **137**, 553–597,
795 doi:10.1002/qj.828.
796
797 Delworth, T. L., and Coauthors, 2006: GFDL's CM2 global coupled climate models. part
798 I: formulation and simulation characteristics. *J. Climate*, **19**, 643-674.
799
800 Douglass, A. R., S. R. Kawa, 1999: Contrast between 1992 and 1997 high-latitude spring
801 Halogen Occultation Experiment observations of lower stratospheric HCL. *J. Geophys.*
802 *Res.,* **104**, 18739-18754.
803
804 Douglass, A. R., R. S. Stolarski, S. E. Strahan, and L. D. Oman, 2012: Understanding
805 differences in upper stratospheric ozone response to changes in chlorine and temperature
806 as computed using CCMVal-2 models. *J. Geophys. Res*., **117**, D16306,
807 doi:10.1029/2012JD017483.
808
809 Downes, S. M., A. M. Hogo, 2013: Southern Ocean circulation and eddy compensation in
810 CMIP5 models. *J. Climate*, **26**, 7198-7220.
811
812 Eyring, V., and Coauthors, 2006: Assessment of temperature, trace species, and ozone in
813 chemistry-climate model simulations of the recent past. *J. Geophys. Res*., **111**, D22308,
814 doi:10.1029/2006JD007327.
815

816 Farneti, R., and T. Delworth, 2010: The role of mesoscale eddies in the remote oceanic
817 response to altered Southern Hemisphere winds. *J. Phys. Oceanogr*., **40**, 2348-2354.
818
819 Gabriel, A., D. Peters, I. Kirchner, and H. F. Graf, 2007: Effect of zonally asymmetric
820 ozone on stratospheric temperature and planetary wave propagation. *Geophys. Res. Lett.*,
821 **34**, L06807, doi:10.1029/2006GL028998.
822
823 Gent, P., and J. McWilliams, 1990: Isopycnal mixing in ocean circulation models. *J.*
824 *Phys. Oceanogr.,* **20**, 150–155.
825
826 Gillett, N. P., and D. W. J. Thompson, 2003: Simulation of recent Southern Hemisphere
827 climate change. *Science*, **302**, 273–275.
828
829 Gillett, N. P., and Coauthors, 2009: Sensitivity of climate to dynamically-consistent zonal
830 asymmetries in ozone. *Geophys. Res. Lett.*, **36**, L10809, doi:10.1029/2009GL037246.
831
832 Griffies, S. M. and Coauthors, 2005: Formulation of an ocean model for global climate
833 simulations. *Ocean Science*, 45-79.
834
835 Griffies, S. M., M. Schmidt, and M. Herzfeld, 2009: Elements of mom4p1. *GFDL Ocean*
836 *Group Tech. Rep*.
837

838 Griffies, M. S., and Coauthors, 2009: Coordinated Ocean-ice Reference Experiments
839 (COREs), *Ocean Modelling*, **26**, 1-46.
840
841 Grytsai, A. V., O. M. Evtushevsky, O. V. Agapitov, A. R. Klekociuk, and G. P.
842 Milinevsky, 2007: Structure and long-term change in the zonal asymmetry in Antarctic
843 total ozone during spring. *Annales. Geophysicae*., **25**, 361-374.
844
845 Hamiberger L., C. Tavolato, and S. Sperka, 2012: Homogenization of the global
846 radiosonde temperature dataset through combined comparison with reanalysis
847 background series and neighboring stations. *J. Climate*, **25**, 8108-8131.
848
849 Hill, C., C. Deluca, Balaji, M. Suarez, A. Da Silva, 2004: The architecture of the Earth
850 System Modeling Framework. *Computing in Science & Engineering*, 18-28.
851
852 Hunke, E. C., and W. H. Lipscomb, 2008: CICE: The Los Alamos Sea Ice Model,
853 Documentation and Software Manual, Version 4.0. Technical Report, Los Alamos
854 National Laboratory.
855
856 Kalnay, E., and Coauthors, 1996: The NCEP/NCAR 40-year reanalysis project. *Bull. Am.*
857 *Meteorol. Soc.*, **77**, 437–471, doi:10.1175/1520-0477.
858

859 Kanamitsu, M., W. Ebisuzaki, J. Woollen, S. K. Yang, J. J. Hnilo, M. Fiorino, and G. L.
860 Potter, 2002: NCEP–DOE AMIP-II reanalysis. *Bull. Am. Meteorol. Soc*., **83**, 1631–1643,
861 doi:10.1175/BAMS-83-11-1631.
862
863 Lauer A., and K. Hamilton, 2013: Simulating clouds with global climate models: a
864 comparison of CMIP5 results with CMIP3 and satellite data. *J. Climate*, **26**, 3823-3845.
865
866 Lee, T., D. E. Waliser,, J. L. F. Li, F. W. Landerer,, and M. M. Gierach, 2013: Evaluation
867 of CMIP3 and CMIP5 wind stress climatology using satellite measurements and
868 atmospheric reanalysis products. *J. Climate*, **26**, 5810-5826.
869
870 Lenton, A., F. Codron, L. Bopp, N. Metzl, P. Cadule, A. Tagliabue, and J. L. Sommer,
871 2009: Stratospheric ozone depletion reduces ocean carbon uptake and enhances ocean
872 acidification. *Geophys. Res. Lett*., **36**, L12606, doi:10.1029/2009GL038227.
873
874 Levitus, S. E., 1982: Climatological atlas of the world ocean. *NOAA Professional paper*
875 **13**, US Government Printing Office, Washington DC.
876
877 Li, F., J. Austin, and J. Wilson, 2008: The strength of the Brewer-Dobson circulation in a
878 changing climate: coupled chemistry-climate simulations. *J. Climate*, **21**, 40-57.
879
880 Marshall, J., and K. Speer, 2012: Closure of the meridional overturning circulation
881 through Southern Ocean upwelling. *Nature Geophys*., **5**, 171-180.

McLandress, C., T. G. Shepherd, S. Polavarapu, and S. R. Beagley, 2011: Is missing orographic gravity wave drag near 60S the cause of the stratospheric zonal wind biases in chemistry-climate models? *J. Climate*, **69**, 802-818.

Molod, A., L. Takacs, M. Suarez, J. Bacmeister, I. S. Song, and A. Eichmann, 2012: The GEOS-5 atmospheric general circulation model: Mean climate and development from MERRA to Fortuna. *Technical Report Series on Global Modeling and Data Assimilation*, **28**, [Available at: http://gmao.gsfc.nasa.gov/pubs/docs/Molod484.pdf.]

Neely, R. R., D. R. Marsh, K. L. Smith, S. M. Davis, and L. M. Polvani, 2014: Biases in southern hemisphere climate trends induced by coarsely specifying the temporal resolution of stratospheric ozone. *Geophys. Res. Lett*., **41**, 8602–8610, doi:10.1002/2014GL061627.

Nathan, T. R., and E. C. Cordero, 2007: An ozone-modified refractive index for vertically propagating planetary waves. *J. Geophys. Res.*, **112**, D02105, doi:10.1029/2006JD007357.

Oman, L. D., and A. R. Douglass, 2014: Improvements in total column ozone in GEOSCCM and comparisons with a new ozone-depleting substances scenario. *J. Geophys. Res.*, **119**, 5613–5624, doi:10.1002/2014JD021590.

905 Pawson, S., R. S. Stolarski, A. R. Douglass, P. A. Newman, J. E. Nielsen, S. M. Frith,
906 and M. L. Gupta, 2008: Goddard Earth Observing System chemistry climate model
907 simulations of stratosphere ozone temperature coupling between 1950 and 2005. *J.*
908 *Geophys. Res*., **113**, D12103, doi:10.1029/2007JD009511.
909
910 Perlwitz, J., S. Pawson, R. L. Fogt, J. E. Nielsen, and W. D. Neff, 2008: Impact of
911 stratospheric ozone hole recovery on Antarctic climate. *Geophys. Res. Lett*., **35**, L08714,
912 doi:10.1029/2008GL033317
913
914 Polvani, L. M., and K. L. Smith, 2013: Can natural variability explain observed Antarctic
915 sea ice trends? New modeling evidence from CMIP5, *Geophys. Res. Lett.*, **40**, 3195–
916 3199, doi:10.1002/grl.50578.
917
918 Previdi, M., and L M. Polvani, 2014: Climate system response to stratospheric ozone
919 depletion and recovery. *Q. J. R. Meteorol. Soc*., doi:10.1002/qj.2330.
920
921 Randel, W. J., and F. Wu, 1999: Cooling of the Arctic and Antarctic polar stratospheres
922 due to ozone depletion. *J. Climate*, **12**, 1467–1479.
923
924 Reynolds, R. W., N. A. Rayner, T. M. Smith, D. C. Stokes, and W. Wang, 2002: An
925 improved in situ and satellite SST analysis for climate. *J. Climate*, **15**, 1609-1625.
926

927 Rienecker, M. M., and Coauthors, 2011. MERRA: NASA's Modern-Era Retrospective
928 Analysis for Research and Applications. *J. Climate,* **24**, 3624-3648, doi:10.1175/JCLI-D-
929 11-00015.1.
930
931 Russell, J. L., K. W. Dixon, A. G. Gnanadesikan, R. J. Stouffer, and J. R. Toggweiler,
932 2006a: The southern hemisphere westerlies in a warming world: propping open the door
933 to the deep ocean. *J. Climate*, **16**, 6382-6390.
934
935 Santer, B., T. Wigley, J. Boyle, D. Gaffen, J. Hnilo, D. Nychka, D. Parker, and K. E.
936 Taylor, 2000: Statistical significance of trends and trend differences in layer-average
937 atmospheric temperature time series. *J. Geophys. Res*., **105**, 7337–7356,
938 doi:10.1029/1999JD901105.
939
940 Sassi, F., B. A. Boville, D. Kinnison, and R. R. Garcia, 2005: The effects of interactive
941 ozone chemistry on simulations of the middle atmosphere. *Geophys. Res. Lett.*, **32**,
942 L07811, doi:10.1029/2004GL022131.
943
944 Sen Gupta, A., A. Santoso, A. S. Taschetto, C. C. Ummenhofer, J. Trevena, and M. H.
945 England, 2009: Projected changes to the Southern Hemisphere ocean and sea ice in the
946 IPCC AP4 climate models. *J. Climate*, **22**, 3047-3078.
947
948 Shine, K. P., 198:. On the modeled thermal response of the Antarctic stratosphere to a
949 depletion of ozone. *Geophys. Res. Lett*., **13**, 1331-1334.

950

951 Sigmond, M., and J. C. Fyfe, 2010: Has the ozone hole contributed to increased Antarctic
952 sea ice extent? *Geophys. Res. Lett.*, **37**, L18502, doi:10.1029/2010GL044301.
953
954 Sigmond, M., J. C. Fyfe, and J. F. Scinocca, 2010: Does the ocean impact the
955 atmospheric response to stratospheric ozone depletion? *Geophys. Res. Lett.*, **37**, L12706,
956 doi:10.1029/2010GL043773.
957
958 Sigmond, M., M. C. Reader, J. C. Fyfe, and N. P. Gillett, 2011: Drivers of past and future
959 Southern Ocean change: Stratospheric ozone versus greenhouse gas impacts. *Geophys.*
960 *Res. Lett*., **38**, L12601, doi:10.1029/2011GL047120.
961
962 Sigmond, M., and J. C. Fyfe, 2014: The Antarctic sea ice response to the ozone hole in
963 climate models. *J. Climate*, **27**, 1336-1342.
964
965 Smith, K. L., L.M. Polvani, and D. R. Marsh, 2012: Mitigation of 21st century Antarctic
966 sea ice loss by stratospheric ozone recovery, *Geophys. Res. Lett.*, **39**, L20701,
967 doi:10.1029/2012GL053325.
968
969 Solomon, A., L. M. Polvani, R. Abernathy and K. L. Smith, 2015: The impact of ozone
970 depleting substances on the circulation, temperature, and salinity of the Southern Ocean:
971 An attribution study with CESM1(WACCM),. *Geophys. Res. Lett*., **42**,
972 DOI:10.1002/2015GL064744.

973

974 Son, S. W., and Coauthors, 2008: The impact of stratospheric ozone recovery on the
975 Southern Hemisphere westerly jet. *Science*, **296**, 895-899.

976

977 Son, S. W., and Coauthors, 2010: Impact of stratospheric ozone on Southern Hemisphere
978 circulation change: A multimodel assessment. *J. Geophys. Res.*, **115**, D00M07,
979 doi:10.1029/2010JD014271.

980

981 Spence, P., J. C. Fyfe, A. Montenegro, and A. J. Weaver, 2010: Southern Ocean response
982 to strengthening winds in an eddy permitting global climate model. *J. Climate*, **23**, 5332–
983 5343.

984

985 SPARC CCMVal, 2010: SPARC Report on the Evaluation of Chemistry-Climate
986 Models, (Eds.), SPARC Report No. 5,WCRP-132, WMO/TD-No. 1526.
987 http://www.atmosp.physics.utoronto.ca/SPARC**.**

988

989 Stolarski, R. S., A. R. Douglass, M. Gupta, P. A. Newman, S. Pawson, M. R. Schoeberl,
990 and J. E. Nielsen, 2006: An ozone increase in the Antarctic summer stratosphere: A
991 dynamical response to the ozone hole, *Geophys. Res. Lett.*, **33**, L21805,
992 doi:10.1029/2006GL026820.

993

994 Strahan, S. E., and Coauthors, 2011: Using transport diagnostics to understand chemistry
995 climate model ozone simulations. *J. Geophys. Res.*, **116**, D17302,
996 doi:10.1029/2010JD015360.
997
998 Swart, N. C., and J. C. Fyfe, 2012: Observed and simulated changes in the Southern
999 Hemisphere surface westerly wind-stress. *Geophys. Res. Lett.*, **39**, L16711,
1000 doi:10.1029/2012GL052810.
1001
1002 Swart, N. C., and J. C. Fyfe, 2013: The influence of recent Antarctic ice sheet retreat on
1003 simulated sea ice area trends, *Geophys. Res. Lett.*, **40**, 4328–4332, doi:10.1002/grl.50820.
1004
1005 Thompson, D. W. J., and J. M. Wallace, 2000: Annular Modes in the extratropical
1006 circulation: Part I: month‐to‐month variability. *J. Climate*, **13**, 1000–1016.
1007
1008 Thompson, D. W. J., and S. Solomon, 2002: Interpretation of recent Southern
1009 Hemisphere climate change. *Science*, **296**, 895–899.
1010
1011 Thompson, D. W. J., S. Solomon, P. J. Kushner, M. H. England, K. M. Grise, and D. J.
1012 Karoly, 2012: Signatures of the Antarctic ozone hole in Southern Hemisphere surface
1013 climate change. *Nature Geosci*., doi:10.1038/NGEO1296.
1014

1015 Turner, J., T. Bracegirdle, T. Phillips, G. Marshall, and J. Hosking, 2013: An initial
1016 assessment of Antarctic sea ice extent in the CMIP5 models. *J. Climate*, **26**, 1473–1484,
1017 doi:10.1175/JCLI-D-12-00068.1.
1018
1019 Waugh, D. W., W. J. Randel, S. Pawson, P. A. Newman, and E. R. Nash, 1999:
1020 Persistence of the lower stratospheric polar vortices. *J. Geophys. Res*., **104**, 27191-27201.
1021
1022 Waugh, D. W., L. Oman, P. A. Newman, R. S. Stolarski, S. Pawson, J. E. Nielsen, and J.
1023 Perlwitz, 2009: Effect of zonal asymmetries in stratospheric ozone on simulated Southern
1024 Hemisphere climate trends. *Geophys. Res. Lett*., **36**, L18701,
1025 doi:10.1029/2009GL040419.
1026
1027 Waugh, D. W., F. Primeau, T. Devries, and M. Holzer, 2013: Recent changes in the
1028 ventilation of the southern oceans. *Science*, **339**, 568-570.
1029
1030 Wigley, T. M. L., 2006: Appendix A: Statistical issues regarding trends. In temperature
1031 trends in the lower atmosphere: steps for understanding and reconciling differences. Karl,
1032 T. R., Hassol, S. J., Miller, C. D., Murray, W. L. (eds). A Report by the U.S. Climate
1033 Change Science Program and the Subcommittee on Global Change Research,
1034 Washington DC.
1035

1036 Zwally, H. J., J. C. Comiso, C. L. Parkinson, D. J. Cavalieri, and P. Gloersen, 2002:
1037 Variability of Antarctic sea ice 1979–1998. *J. Geophys. Res*., **107**, 3041.
1038 doi:10.1029/2000JC000733.
1039
1040

Figure captions

Figure 1: Zonal-mean total column ozone distributions in 1990-2010 as a function of month and latitude. (a) GEOS AOCCM interactive chemistry simulations. (b) Merged SBUV/TOMS total ozone data. Contour interval is 25 Dobson Unit. No observations in polar night.

Figure 2: (a) Climatological seasonal cycle of Antarctic zonal-mean temperatures (averaged over 65°S to 90°S) in 1990-2010 in the GEOS AOCCM simulations and (b) the differences between the simulations and MERRA reanalysis. (c) Climatological seasonal cycle of Antarctic circumpolar zonal-mean zonal winds (averaged over 55°S to 70°S) in the AOCCM simulations and (d) the differences between the simulations and MERRA. (e) Climatological annual-mean zonal-mean zonal winds in the Southern Hemisphere in the AOCCM simulations and (f) the differences between the simulations and MERRA.

Figure 3: (a) Annual-mean zonal surface wind-stress climatology in 1990-2010 in the GEOS AOCCM simulations. (b) Zonal wind-stress climatology differences between GEOS AOCCM simulations and the Quick Scatterometer (QuikSCAT) observations. (c) Zonal-mean zonal wind-stress climatology in the Southern Hemisphere in the QuikSCAT (black solid), reanalysis (black dashed), and GEOS AOCCM simulations (green). The reanalysis data is the average of four datasets: MERRA, NCEP-NCAR, NCEP-DOE, and ERA-Interim. Shading shows the standard deviation of the four reanalyses climatology.

1064

1065 Figure 4: (a) Annual-mean sea surface temperature (SST) climatology in 1990-2010 in
1066 the GEOS AOCCM simulations and (b) the differences between the modeled SST and
1067 Reynolds data. (c) Annual-mean sea surface salinity (SSS) climatology in 1990-2010 in
1068 the GEOS AOCCM simulations and (d) the differences between the modeled SSS and
1069 Levitus data.

1070

1071 Figure 5: (a) Climatological Southern Ocean annual-mean Eulerian Meridional
1072 Overturning Circulation (MOC) streamfunction in 1990-2010 in the GEOS AOCCM
1073 simulations. (b) Same as (a), but for the parameterized eddy MOC streamfunction.
1074 Contour interval is 4 and 2 Sv for the Eulerian and eddy streamfunction, respectively.

1075

1076 Figure 6: Climatological Antarctic sea ice extent seasonal cycle in 1990-2010 in the
1077 GEOS AOCCM simulations (green) and the National Snow and Ice Data Center
1078 observations (black).

1079

1080 Figure 7: (a) Climatological seasonal cycle of Antarctic total ozone (averaged over 65°S
1081 to 90°S) in 1990-2010 for SBUV/TOMS (black), interactive chemistry (green) and
1082 prescribed ozone (red) simulations. (b) Zonal standard deviations of Antarctic ozone
1083 (averaged over 65°S to 90°S) in the interactive chemistry simulations.

1084

1085 Figure 8: Differences in Antarctic (a) temperature, (b) ozone, (c) dynamical heating and
1086 (d) shortwave heating rate (averaged over 65°S to 90°S and 1990-2010) between the

1087 interactive chemistry and prescribed ozone simulations (interactive minus prescribed).
1088 Shading indicates that the differences are statistically significant at the 5% level based on
1089 a two-sample t-test.
1090
1091 Figure 9: (a-c) Linear trends of Antarctic zonal-mean temperatures (65°S-90°S) in 1979-
1092 2010 in the interactive simulations, prescribed simulations, and MERRA. Unit is
1093 K/decade. (d-f) Same as (a-c), but for the circumpolar zonal-mean zonal winds (55°S-
1094 70°S). Unit is m/s/decade. (g-h) Linear trends of Antarctic shortwave heating rates (65°S-
1095 90°S) in 1979-2010 in the interactive and prescribed simulations. Unit is K/decade. (i-j)
1096 Same as (g-h), but for the dynamical heating rates. Shading indicates that the trends are
1097 statistically significant at 5% level.
1098
1099 Figure 10: Monthly surface zonal wind trends (averaged over 55°S to 70°S) in 1979-2010
1100 in the interactive chemistry (green) and prescribed ozone (red) simulations. Error bars
1101 (95% confidence interval) in the interactive and prescribed simulations are slightly offset
1102 to show their differences. Filled circles indicate that the trends are statistically significant
1103 at the 5% level.
1104
1105 Figure 11: Linear trends of November-December-January zonal-mean zonal wind in
1106 1979-2010 in (a) interactive chemistry simulations and (b) prescribed ozone simulations.
1107 Unit is m/s/decade. The trends with magnitude of greater than about 0.25 m/s/decade are
1108 statistically significant at the 2-tailed 5% level. Shading indicates that the trends in the

1109 interactive simulations are significantly stronger than those in the prescribed simulations
1110 at the 5% level using a one-tailed t test.
1111
1112 Figure 12: (a) Trends of the November-December-January zonal-mean surface zonal
1113 wind-stress in 1979-2010. Green and red lines are results from the interactive chemistry
1114 and prescribed ozone simulations, respectively. Solid lines represent that the trends are
1115 statistically significant from zero at the 95% confidence interval. Asterisks indicate where
1116 the trends in the interactive simulations are significantly stronger than those in the
1117 prescribed simulations.. (b) Trends of the NDJ maximum surface zonal wind-stress in the
1118 Southern Hemisphere in 1979-2010. The error bars show the 95% confidence interval.
1119
1120 Figure 13: (a) Trends of the November-December-January zonal-mean zonal surface
1121 ocean currents in 1979-2010 in the interactive chemistry (green) and prescribed ozone
1122 (red) simulations. Solid lines represent that the trends are statistically significant from
1123 zero at the 95% confidence interval. Asterisks indicate where the trends in the interactive
1124 simulations are significantly stronger than those in the prescribed simulations. (b) Same
1125 as (a), but for the meridional surface currents. (c) Trends of the NDJ zonal-mean zonal
1126 ocean currents in 1979-2010 in the interactive simulations. (d) Same as (c), but for the
1127 prescribed simulations. Trends with magnitude larger than 0.05 cm/s/decade are
1128 statistically significant from zero. Shading in (c) and (d) indicates where the zonal current
1129 trends in the interactive simulations are significantly stronger than those in the prescribed
1130 simulations at the 1-tailed 5% level. (e) Trends of the NDJ zonal-mean meridional ocean
1131 currents in 1979-2010 in the interactive simulations. (f) Same as (e), but for prescribed

1132 simulations. Shading in (e) and (f) indicates where the meridional current trends in the
1133 interactive simulations are significantly stronger than those in the prescribed simulations
1134 at the 1-tailed 5% level. Unit in all panels is cm/s/decade.
1135
1136 Figure 14: Trends of the November-December-January Southern Ocean MOC
1137 streamfunction in 1979-2010 in (a) interactive chemistry and (b) prescribed ozone
1138 simulations. Poleward of 55°S, trends with magnitude grater than about 0.3 Sv/decade
1139 are statistically significant from zero at the 2-tailed 5% level. Equatorward of 55°S,
1140 trends with magnitude greater than about 0.6 Sv/decade are statistically significant.
1141 Shading indicates where the MOC trends in the interactive simulations are significantly
1142 stronger than those in the prescribed simulations at the 1-tailed 5% level. Unit of the
1143 trends is Sv/decade.
1144
1145 Figure 15: (Top) Trends of the zonal-mean ocean temperature in 1979-2010 (color
1146 shading) and climatology in 1990-2010 (contours) in (a) November-December-January
1147 and (b) May-June-July in the interactive chemistry simulations. Trends are statistically
1148 significant from zero at the 2-tailed 5% level poleward of 45°S except for the very weak
1149 surface cooling near 64°S. Equatorward of 45°S, trends with magnitude greater than
1150 about 0.15 °C/decade are statistically significant. Units of the trends (color shading) and
1151 climatology (contours) are respectively °C/decade and °C. (Bottom) Differences in zonal-
1152 mean ocean temperature trends between the interactive chemistry and prescribed ozone
1153 simulations in (c) November-December-January and (d) May-June-July. Unit is
1154 °C/decade. Shading indicates where the trends in the interactive simulations are

1155 significantly larger than those in prescribed simulations. Note that the depth ranges are
1156 different in the top and bottom panels.
1157
1158 Figure 16: Monthly trends of the Antarctic sea ice extent in 1979-2010 in the interactive
1159 chemistry (green) and prescribed ozone (red) simulations. Error bars are the 95%
1160 confidence interval of the trends. Filled circles indicate that the trends are statistically
1161 significant at the 5% level.

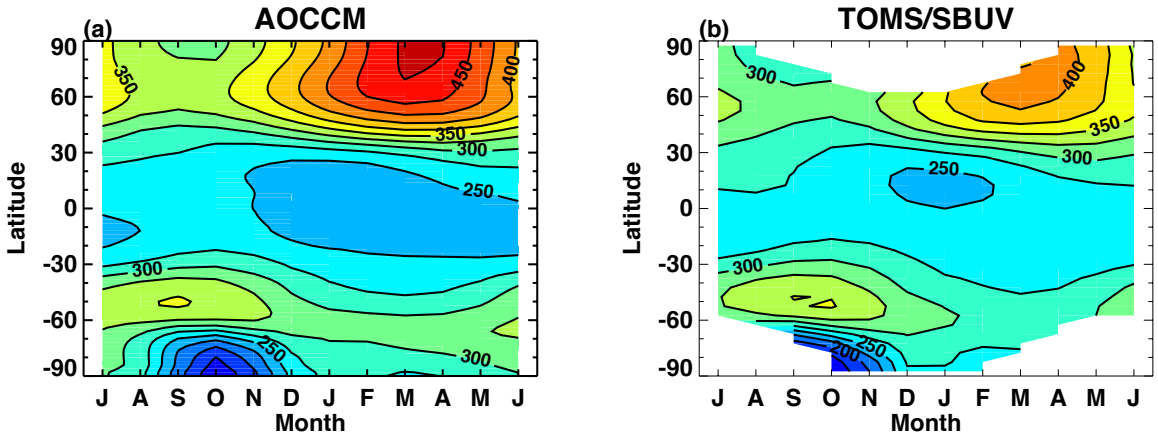

1162

1163 Figure 1: Zonal-mean total column ozone distributions in 1990-2010 as a function of

1164 month and latitude. (a) GEOS AOCCM interactive chemistry simulations. (b) Merged

1165 SBUV/TOMS total ozone data. Contour interval is 25 Dobson Unit. No observations in

1166 polar night.

1167

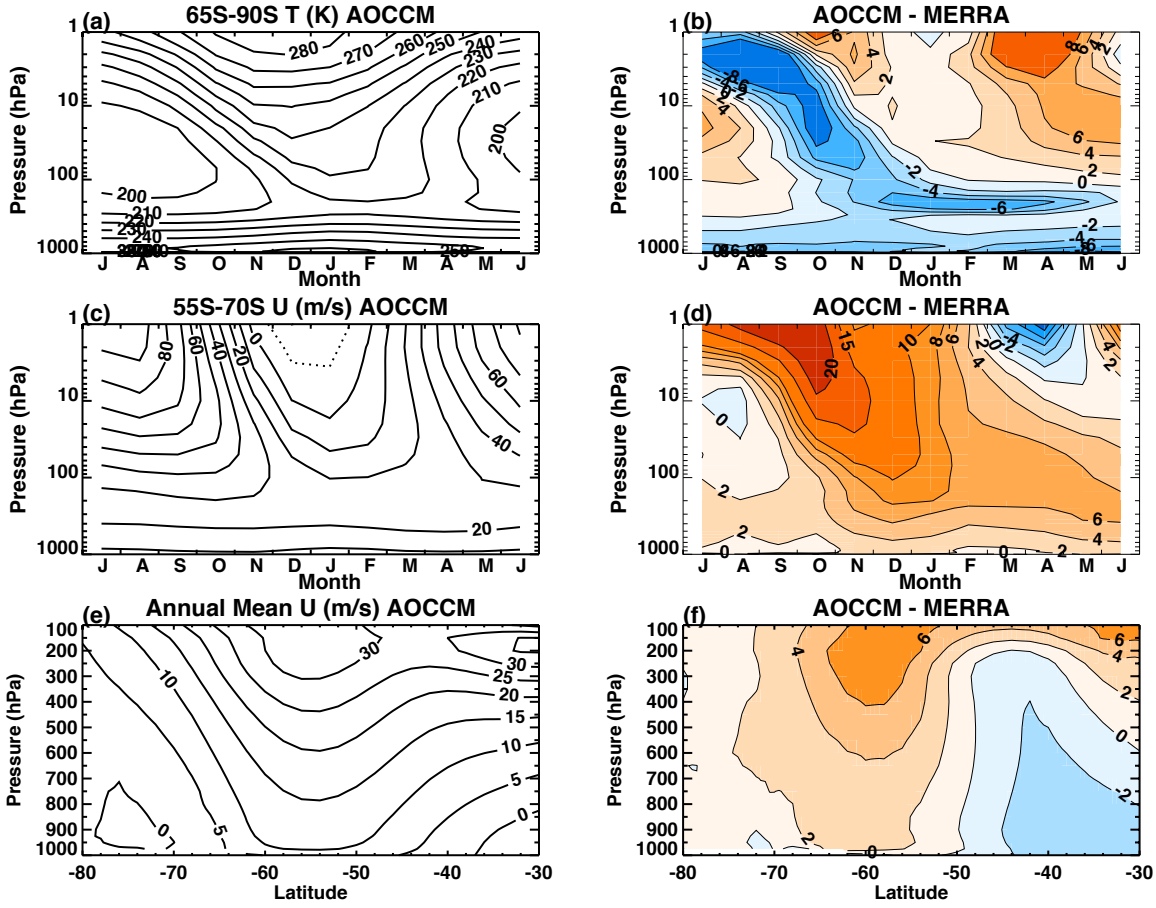

1168

1169 Figure 2: (a) Climatological seasonal cycle of Antarctic zonal-mean temperatures
1170 (averaged over 65°S to 90°S) in 1990-2010 in the GEOS AOCCM simulations and (b)
1171 the differences between the simulations and MERRA reanalysis. (c) Climatological
1172 seasonal cycle of Antarctic circumpolar zonal-mean zonal winds (averaged over 55°S to
1173 70°S) in the AOCCM simulations and (d) the differences between the simulations and
1174 MERRA. (e) Climatological annual-mean zonal-mean zonal winds in the Southern
1175 Hemisphere in the AOCCM simulations and (f) the differences between the simulations
1176 and MERRA.

1177

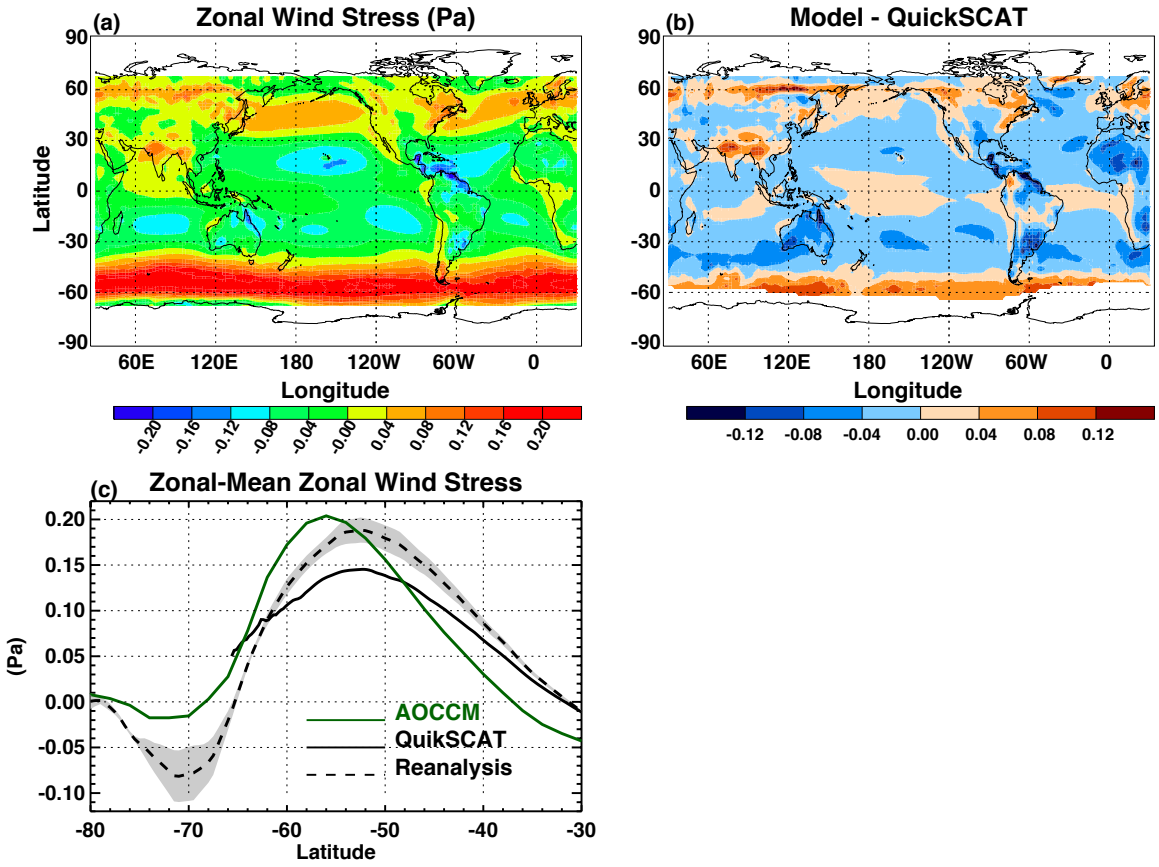

1178

1179 Figure 3: (a) Annual-mean zonal surface wind-stress climatology in 1990-2010 in the
1180 GEOS AOCCM simulations. (b) Zonal wind-stress climatology differences between
1181 GEOS AOCCM simulations and the Quick Scatterometer (QuikSCAT) observations. (c)
1182 Zonal-mean zonal wind-stress climatology in the Southern Hemisphere in the QuikSCAT
1183 (black solid), reanalysis (black dashed), and GEOS AOCCM simulations (green). The
1184 reanalysis data is the average of four datasets: MERRA, NCEP-NCAR, NCEP-DOE, and
1185 ERA-Interim. Shading shows the standard deviation of the four reanalyses climatology.

1186

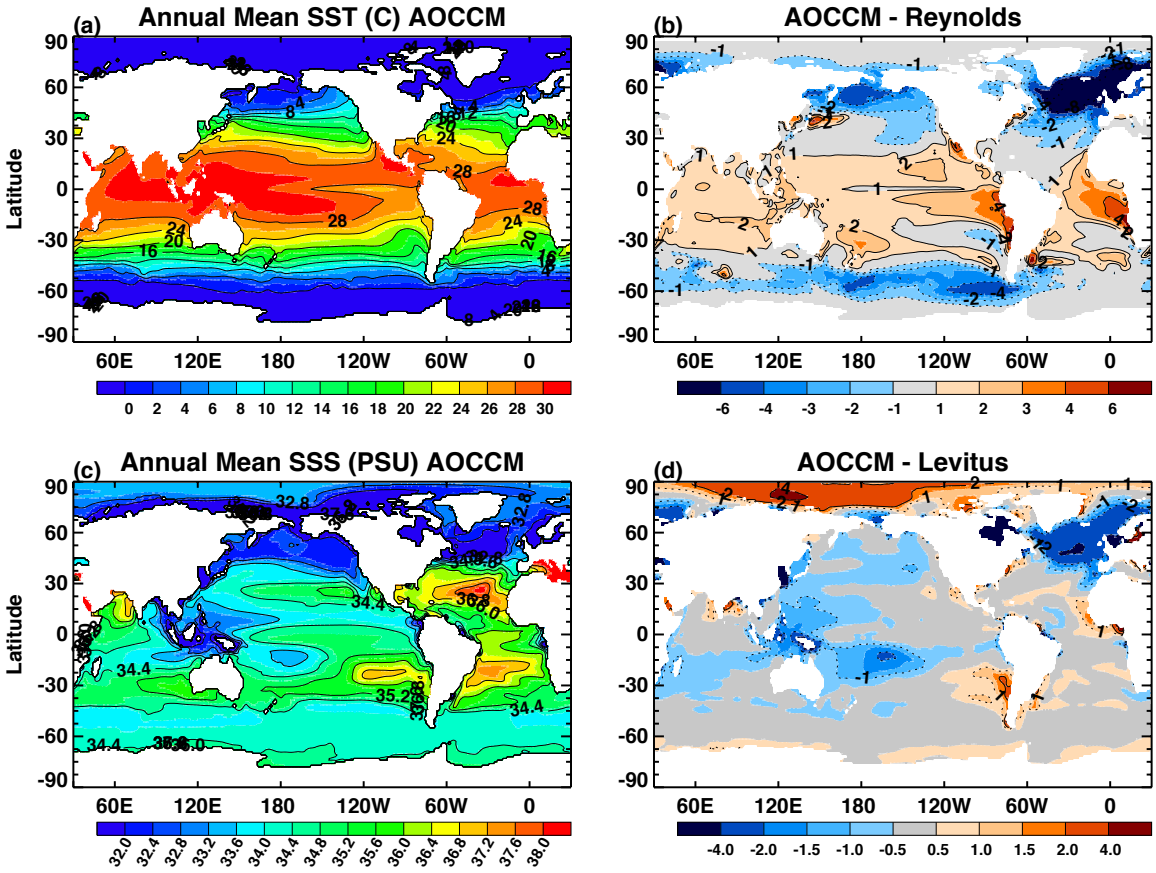

1187

1188 Figure 4: (a) Annual-mean sea surface temperature (SST) climatology in 1990-2010 in

1189 the GEOS AOCCM simulations and (b) the differences between the modeled SST and

1190 Reynolds data. (c) Annual-mean sea surface salinity (SSS) climatology in 1990-2010 in

1191 the GEOS AOCCM simulations and (d) the differences between the modeled SSS and

1192 Levitus data.

1193

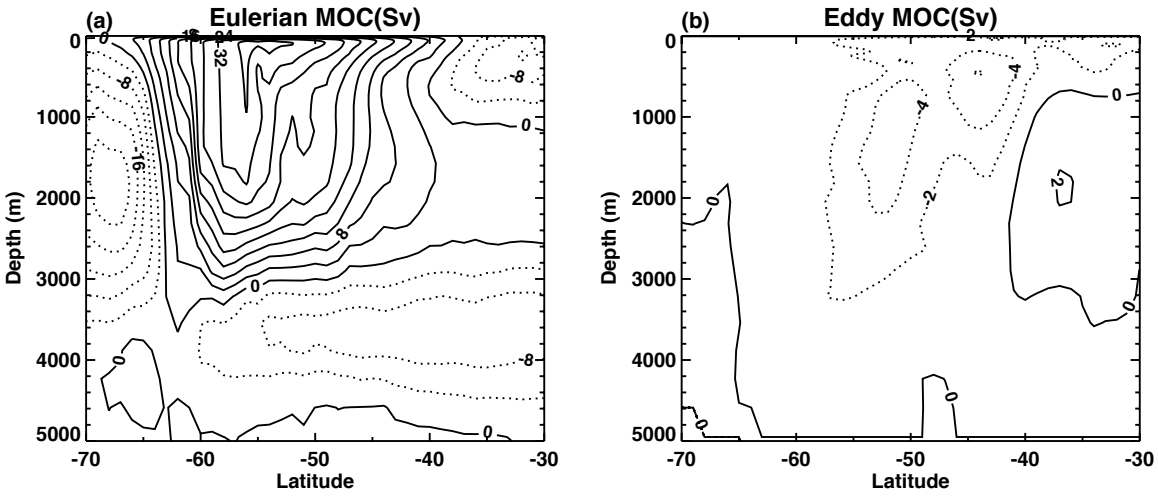

Figure 5: (a) Climatological Southern Ocean annual-mean Eulerian Meridional Overturning Circulation (MOC) streamfunction in 1990-2010 in the GEOS AOCCM simulations. (b) Same as (a), but for the parameterized eddy MOC streamfunction. Contour interval is 4 and 2 Sv for the Eulerian and eddy streamfunction, respectively.

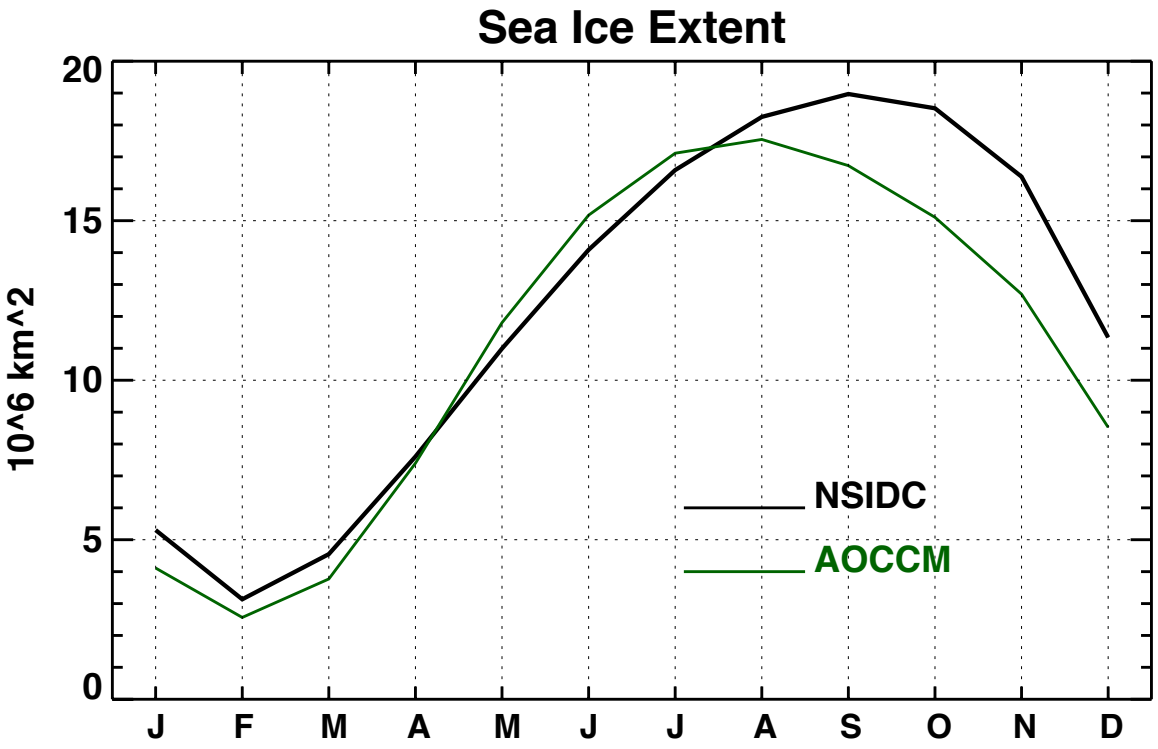

Figure 6: Climatological Antarctic sea ice extent seasonal cycle in 1990-2010 in the GEOS AOCCM simulations (green) and the National Snow and Ice Data Center observations (black).

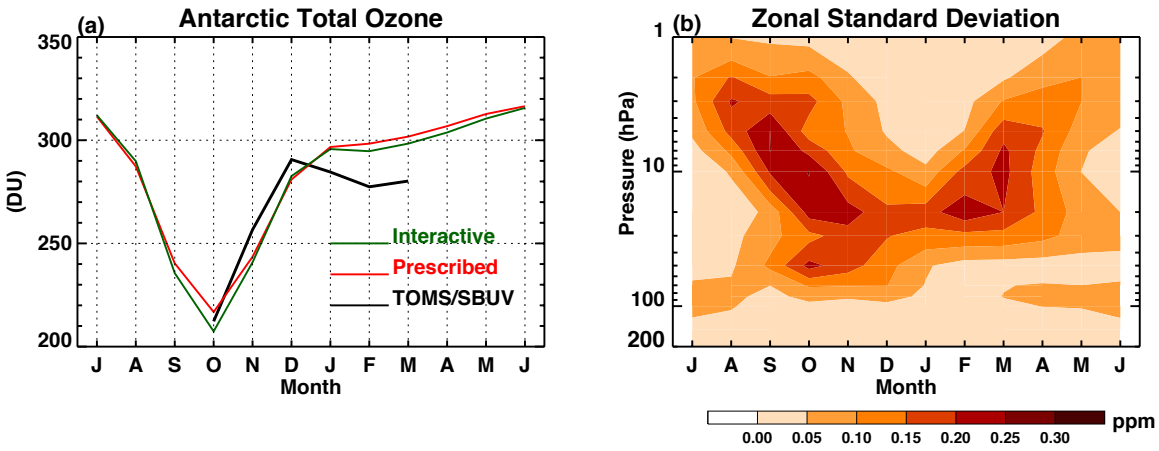

1205

1206 Figure 7: (a) Climatological seasonal cycle of Antarctic total ozone (averaged over 65°S

1207 to 90°S) in 1990-2010 for SBUV/TOMS (black), interactive chemistry (green) and

1208 prescribed ozone (red) simulations. (b) Zonal standard deviations of Antarctic ozone

1209 (averaged over 65°S to 90°S) in the interactive chemistry simulations.

1210

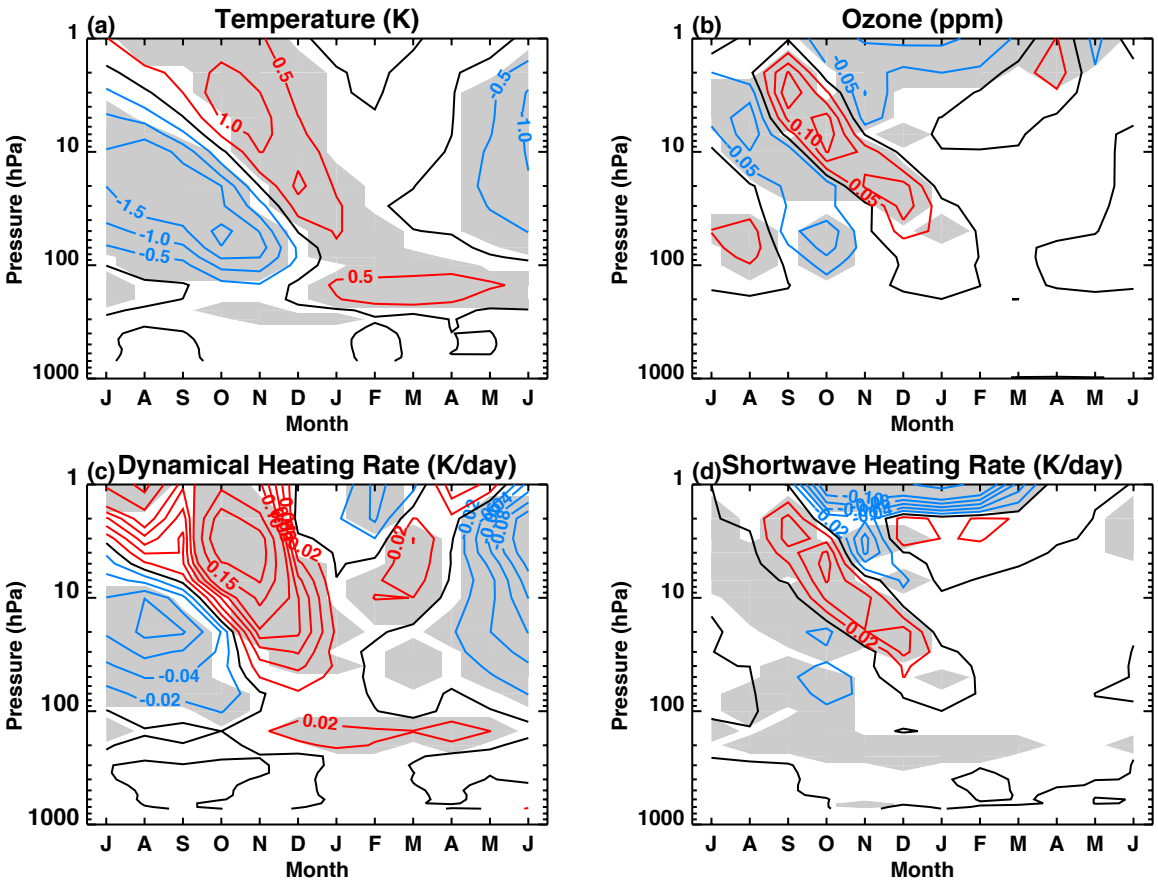

1211

1212 Figure 8: Differences in Antarctic (a) temperature, (b) ozone, (c) dynamical heating and

1213 (d) shortwave heating rate (averaged over 65°S to 90°S and 1990-2010) between the

1214 interactive chemistry and prescribed ozone simulations (interactive minus prescribed).

1215 Shading indicates that the differences are statistically significant at the 5% level based on

1216 a two-sample t-test.

1217

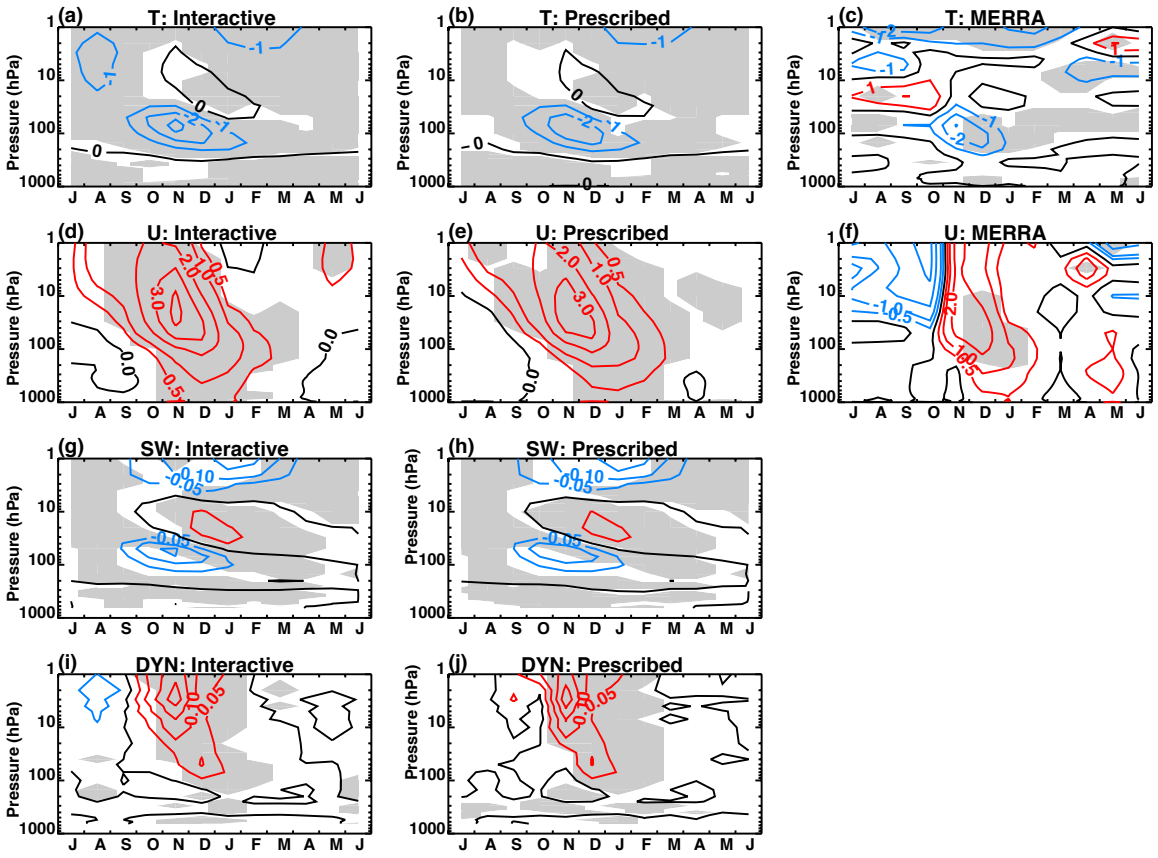

1218

1219 Figure 9: (a-c) Linear trends of Antarctic zonal-mean temperatures (65°S-90°S) in 1979-

1220 2010 in the interactive simulations, prescribed simulations, and MERRA. Unit is

1221 K/decade. (d-f) Same as (a-c), but for the circumpolar zonal-mean zonal winds (55°S-

1222 70°S). Unit is m/s/decade. (g-h) Linear trends of Antarctic shortwave heating rates (65°S-

1223 90°S) in 1979-2010 in the interactive and prescribed simulations. Unit is K/decade. (i-j)

1224 Same as (g-h), but for the dynamical heating rates. Shading indicates that the trends are

1225 statistically significant at 5% level.

1226

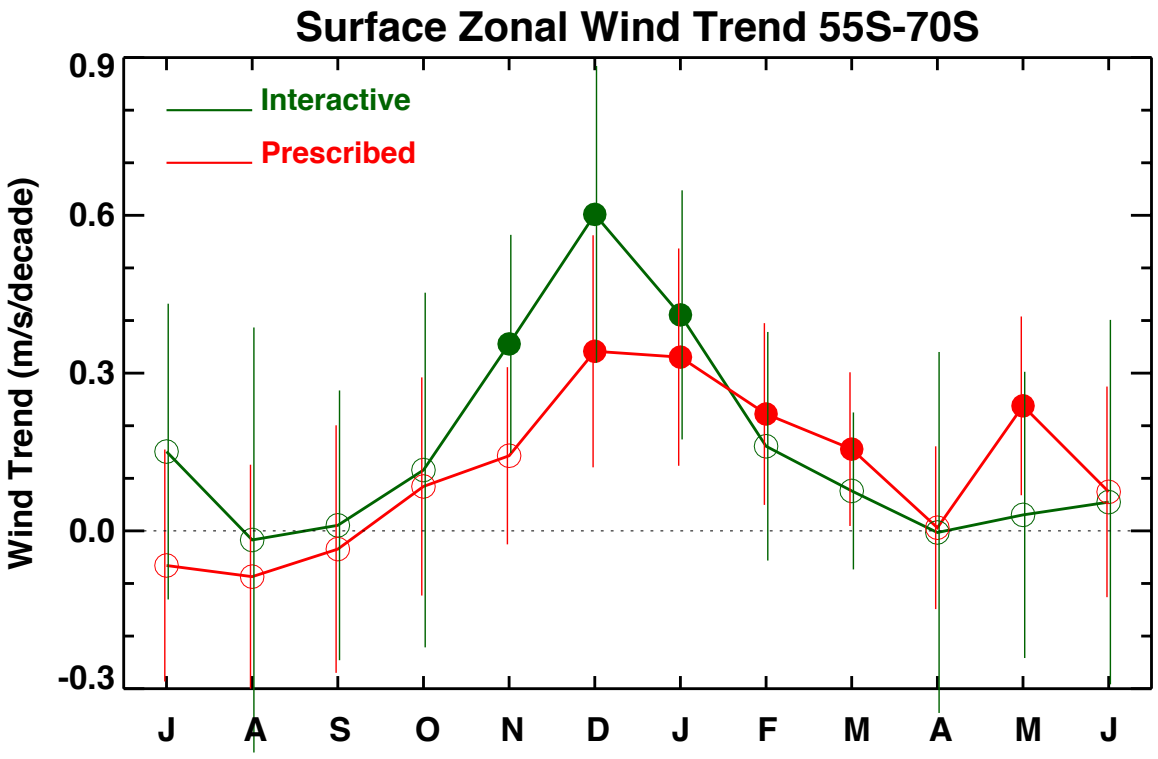

Figure 10: Monthly surface zonal wind trends (averaged over 55°S to 70°S) in 1979-2010 in the interactive chemistry (green) and prescribed ozone (red) simulations. Error bars (95% confidence interval) in the interactive and prescribed simulations are slightly offset to show their differences. Filled circles indicate that the trends are statistically significant at the 5% level.

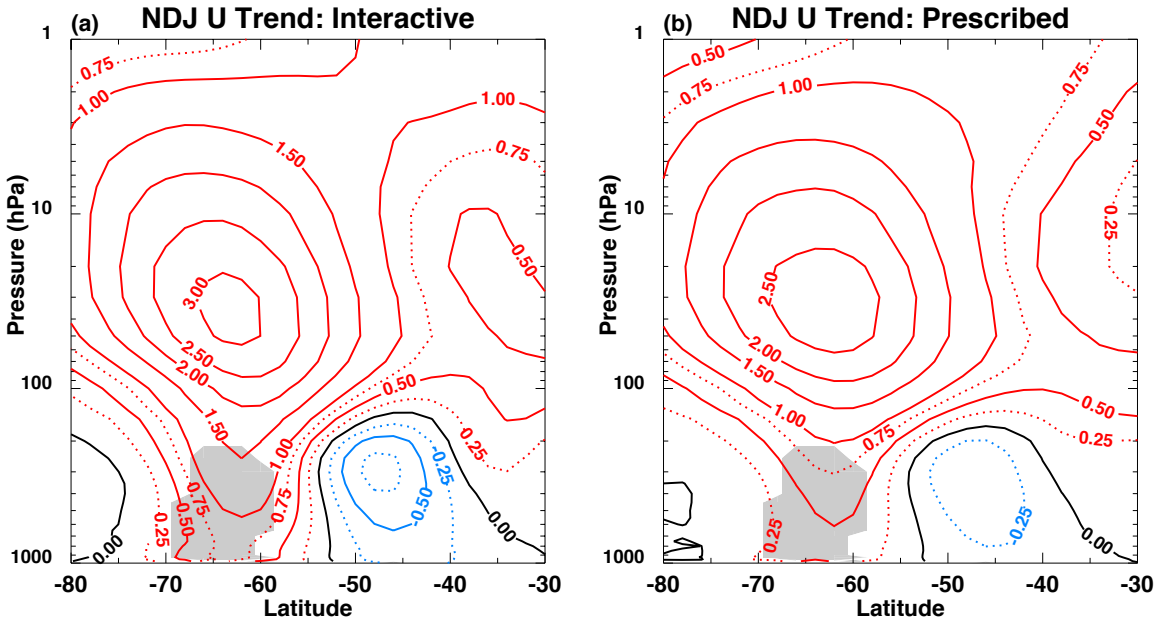

Figure 11: Linear trends of November-December-January zonal-mean zonal wind in 1979-2010 in (a) interactive chemistry simulations and (b) prescribed ozone simulations. Unit is m/s/decade. The trends with magnitude of greater than about 0.25 m/s/decade are statistically significant at the 2-tailed 5% level. Shading indicates that the trends in the interactive simulations are significantly stronger than those in the prescribed simulations at the 5% level using a one-tailed t test.

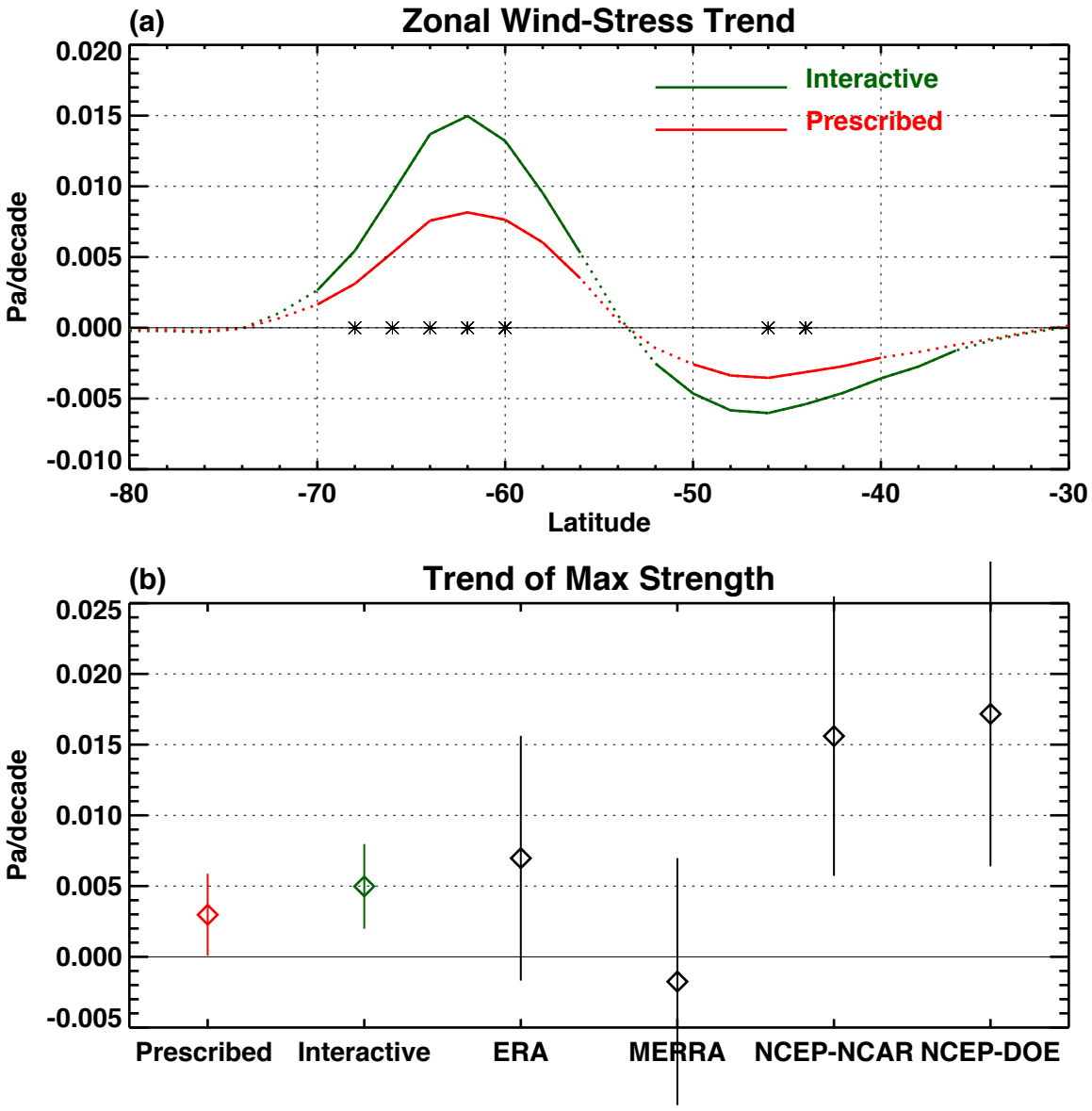

Figure 12: (a) Trends of the November-December-January zonal-mean surface zonal wind-stress in 1979-2010. Green and red lines are results from the interactive chemistry and prescribed ozone simulations, respectively. Solid lines represent that the trends are statistically significant from zero at the 95% confidence interval. Asterisks indicate where the trends in the interactive simulations are significantly stronger than those in the prescribed simulations. (b) Trends of the NDJ maximum surface zonal wind-stress in the Southern Hemisphere in 1979-2010. The error bars show the 95% confidence interval.

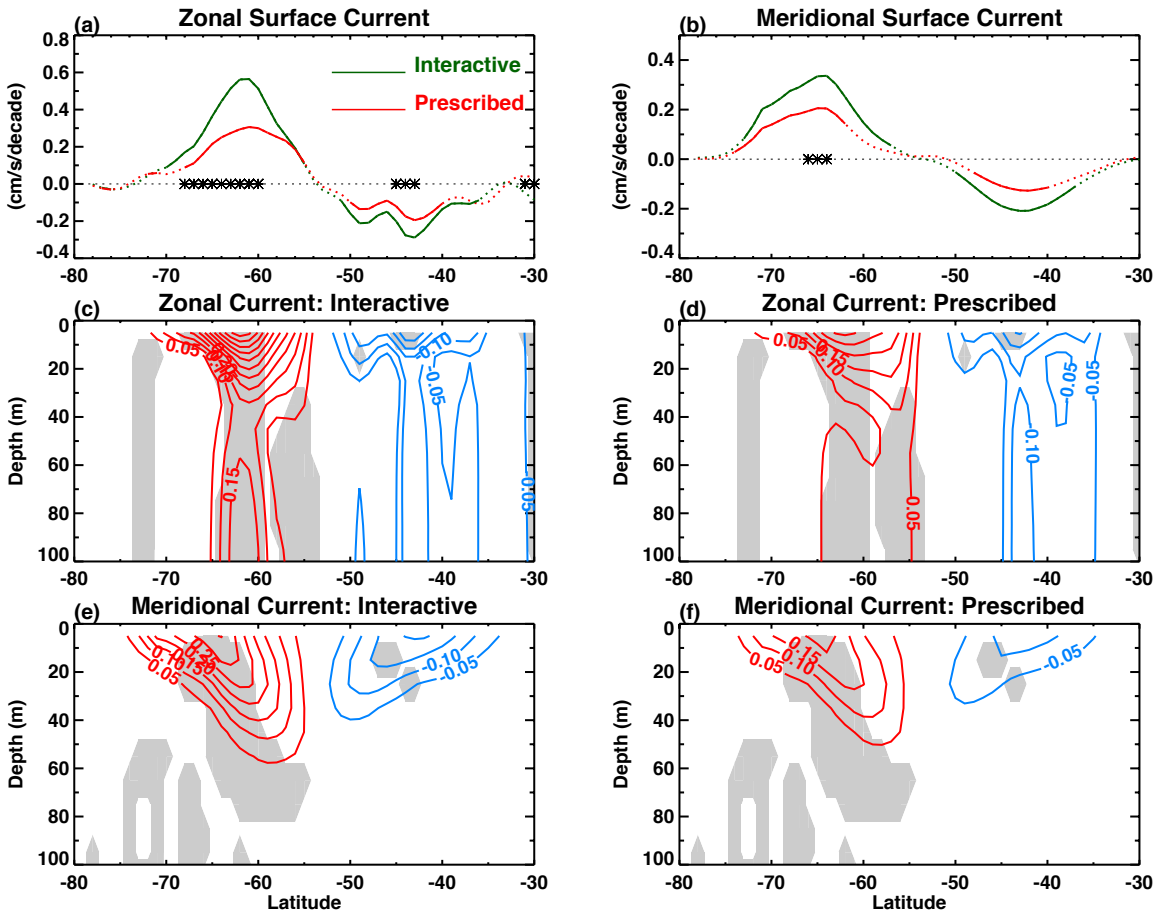

Figure 13: (a) Trends of the November-December-January zonal-mean zonal surface ocean currents in 1979-2010 in the interactive chemistry (green) and prescribed ozone (red) simulations. Solid lines represent that the trends are statistically significant from zero at the 95% confidence interval. Asterisks indicate where the trends in the interactive simulations are significantly stronger than those in the prescribed simulations. (b) Same as (a), but for the meridional surface currents. (c) Trends of the NDJ zonal-mean zonal ocean currents in 1979-2010 in the interactive simulations. (d) Same as (c), but for the prescribed simulations. Trends with magnitude larger than 0.05 cm/s/decade are statistically significant from zero. Shading in (c) and (d) indicates where the zonal current trends in the interactive simulations are significantly stronger than those in the prescribed simulations at the 1-tailed 5% level. (e) Trends of the NDJ zonal-mean meridional ocean

currents in 1979-2010 in the interactive simulations. (f) Same as (e), but for prescribed simulations. Shading in (e) and (f) indicates where the meridional current trends in the interactive simulations are significantly stronger than those in the prescribed simulations at the 1-tailed 5% level. Unit in all panels is cm/s/decade.

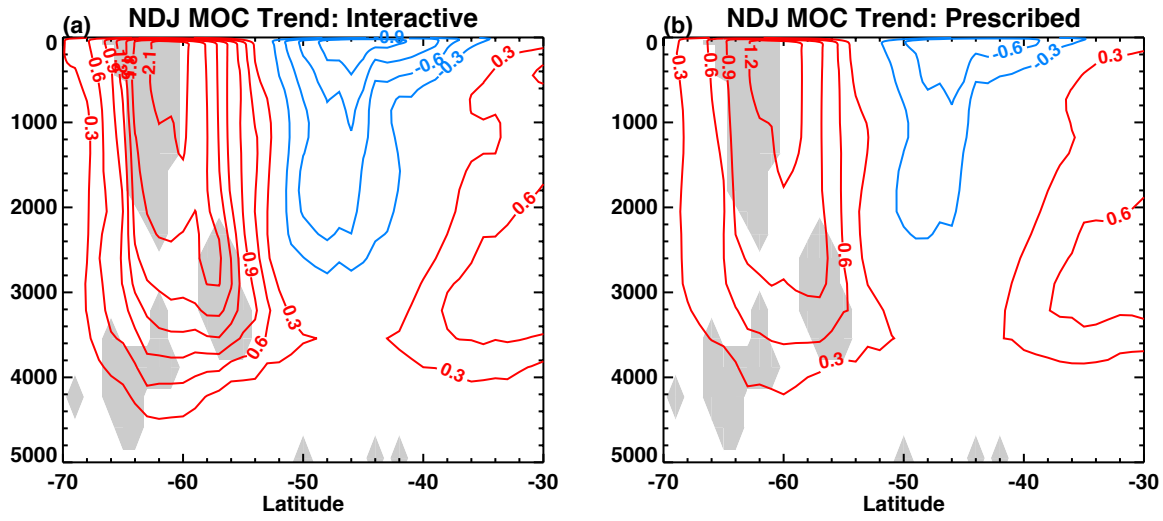

1267

1268 Figure 14: Trends of the November-December-January Southern Ocean MOC
1269 streamfunction in 1979-2010 in (a) interactive chemistry and (b) prescribed ozone
1270 simulations. Poleward of 55°S, trends with magnitude grater than about 0.3 Sv/decade
1271 are statistically significant from zero at the 2-tailed 5% level. Equatorward of 55°S,
1272 trends with magnitude greater than about 0.6 Sv/decade are statistically significant.
1273 Shading indicates where the MOC trends in the interactive simulations are significantly
1274 stronger than those in the prescribed simulations at the 1-tailed 5% level. Unit of the
1275 trends is Sv/decade.

1276

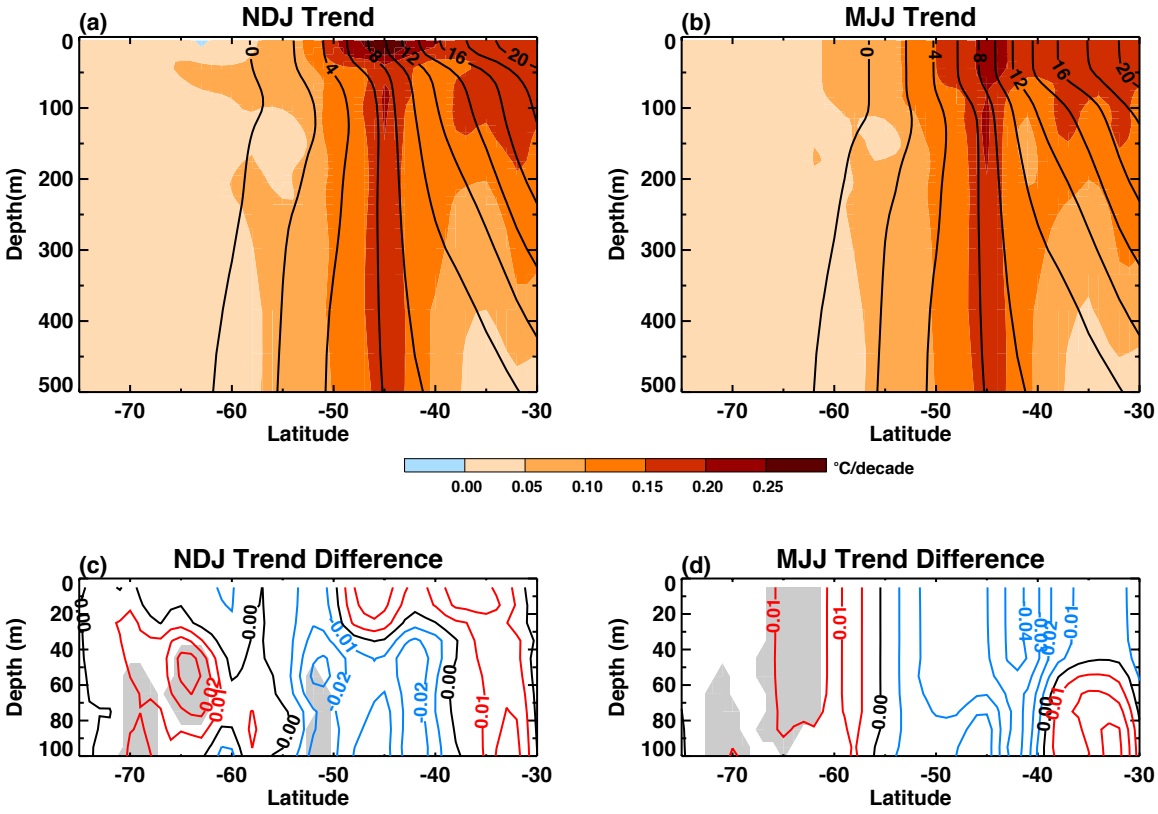

1277

1278 Figure 15: (Top) Trends of the zonal-mean ocean temperature in 1979-2010 (color
1279 shading) and climatology in 1990-2010 (contours) in (a) November-December-January
1280 and (b) May-June-July in the interactive chemistry simulations. Trends are statistically
1281 significant from zero at the 2-tailed 5% level poleward of 45°S except for the very weak
1282 surface cooling near 64°S. Equatorward of 45°S, trends with magnitude greater than
1283 about 0.15 °C/decade are statistically significant. Units of the trends (color shading) and
1284 climatology (contours) are respectively °C/decade and °C. (Bottom) Differences in zonal-
1285 mean ocean temperature trends between the interactive chemistry and prescribed ozone
1286 simulations in (c) November-December-January and (d) May-June-July. Unit is
1287 °C/decade. Shading indicates where the trends in the interactive simulations are
1288 significantly larger than those in prescribed simulations. Note that the depth ranges are
1289 different in the top and bottom panels.

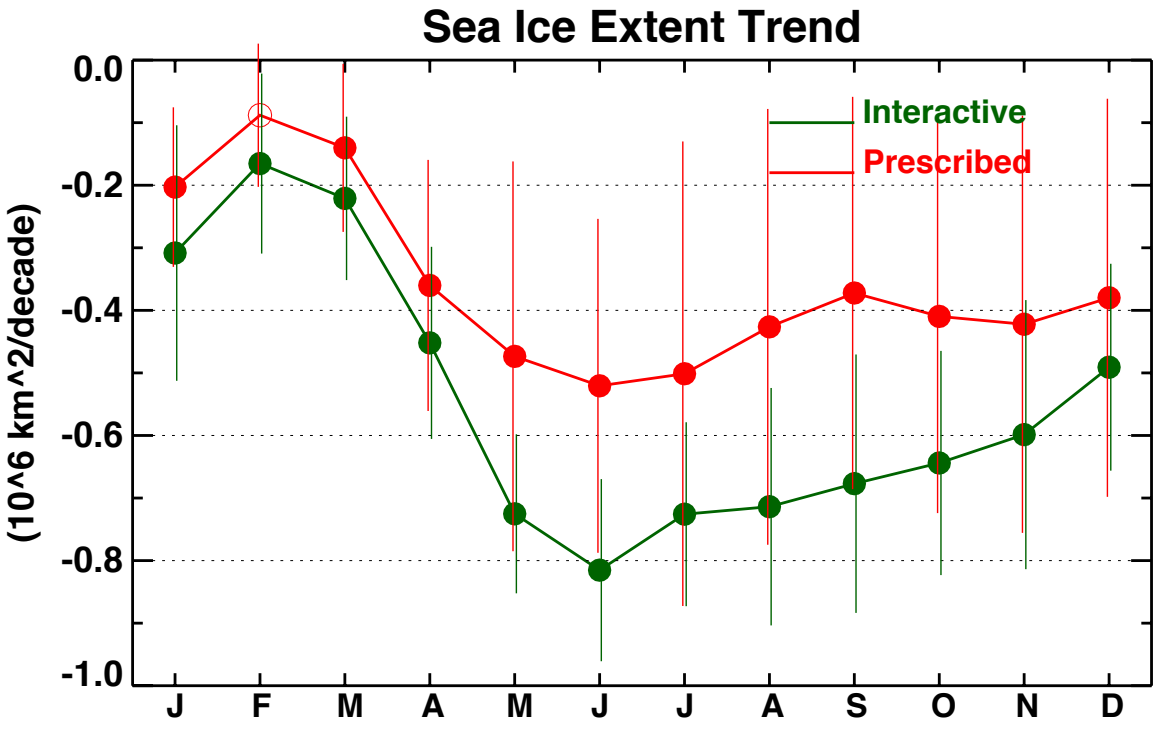

Figure 16: Monthly trends of the Antarctic sea ice extent in 1979-2010 in the interactive chemistry (green) and prescribed ozone (red) simulations. Error bars are the 95% confidence interval of the trends. Filled circles indicate that the trends are statistically significant at the 5% level.